CENTER FOR ASTROPHYSICS
HARVARD & SMITHSONIAN

Submillimeter Array Newsletter

Number 32, July 2021

CONTENTS

FROM THE DIRECTOR

Dear SMA Newsletter readers,

This past year has been a difficult year, and maintaining SMA operations to the highest standard has been, and continues to be, challenging. Since the onset of the pandemic more than a year ago, in common with many organizations, performing certain routine maintenance tasks and effecting repairs to damaged or failing equipment became infeasible in part due to safety restrictions implemented for staff working in close proximity. As a result, the SMA has not been able to sustain science observations with the full eight-element array for some time. While we currently have only six antennas in the array, with two antennas off-line with antenna drive-system issues, we have imposed modifications to observing strategy, coupled with postponing the most demanding high fidelity, high resolution observations, which has enabled science observations to continue.

The antenna drive-system issues are well understood, and I am confident that the dedicated staff at the observatory site will resolve the current issues in the next several weeks. As a result, the SMA call for proposals will offer the full-range of observation types for the upcoming 2022A semester (deadline of 16 September). However, we acknowledge that some users may have been adversely affected by the SMA's reduced capability, and would encourage those PIs whose projects were impacted to please contact SMA TAC chair for guidance on proposal resubmission, or additional observing time.

Raymond Blundell

MULTI-EPOCH SMA OBSERVATIONS OF THE L1448C(N) PROTOSTELLAR JET

Tomohiro Yoshida,[1, 2, 3] Tien-Hao Hsieh,[4, 5] Naomi Hirano,[4] and Yusuke Aso[6]

Protostellar jets/outflows are ubiquitous in star forming regions. Jets/outflows are considered to be playing a crucial role in mass accretion; they remove excess angular momentum and enable the material around protostar to accrete onto the star (e.g., Lee 2020).

L1448C(N), a class 0 protostar with a luminosity of ~14 $L_{\odot}$ (Tobin et al. 2007), at the distance of 293 pc (Ortiz-Léon et al. 2018) in the Perseus molecular cloud complex, drives an archetypical outflow with an extremely high-velocity (EHV) jet (Bachiller et al. 1991; Hirano et al. 2010) and is one of the excellent examples to study protostellar jets/outflows. The EHV components have been detected through several transitions of silicon monoxide (SiO) and carbon monoxide (CO) (e.g., Bachiller et al. 1991; Nisini et al. 2007; Hirano et al. 2010). Hirano et al. (2010) reported high-angular resolution observations of the SiO J=8–7 and CO J=3–2 with the Submillimeter Array (SMA). They found that the highly-collimated jet traced by SiO and CO consists of a chain of knots and is running along the axes of the V-shaped cavities traced by the CO at a lower velocity. They found that the mechanical power of the jet is comparable to the bolometric luminosity of the central source, and concluded that the jet in L1448C(N) is 'extremely active', which suggests the extremely youth of the central protostar.

However, the derived parameters including mechanical power strongly depend on the inclination angle of jets. In the previous estimation, Hirano et al. (2010) adopted the inclination angle of 21° with respect to the plane of the sky derived by Girart & Acord (2001); this is based on the proper motion of the SiO clumps together with the radial velocity measured with the Plateau de Bure Interferometer and the Berkeley-Illinois-Maryland Association Millimeter Array. Since the angular resolution of these observations were ~3″, which is larger than the jet knots resolved by SMA, the derived inclination angle had a large uncertainty.

We have measured the proper motion of the L1448C(N) protostellar jet using the three epoch SiO J = 8 − 7 data observed in 2006, 2010, and 2017 with the SMA at an angular resolution of ~1″.

Figure 1 shows the high-velocity SiO jet observed in 2010. The highly collimated jet consists of several knots. The position angle of the jet is ~−25° in the blueshifted component, while it is ~−18° in the redshifted component. Figure 2 compares the EHV jets at the three epochs. The images are rotated counterclockwise by 25° and 18°. We measured the positions and the velocity offsets of the knots on the position-velocity (PV) diagram of each epoch (Figure 3). The derived positions of the knots on the plane of the sky are plotted on Figure 2, which clearly shows that the knots are moving toward the downstream of the jets. The averaged proper motions are ~0".06 yr^{-1} in the blueshifted jet and ~0″.04 yr^{-1} in the redshifted jet. The corresponding transverse velocities are ~78 km s^{-1} and ~52 km s^{-1} for the blue- and redshifted jet, respectively. The transverse and radial velocities of each knot are plotted in Figure 4. On this plot, the inclination angles of the jets from the plane of the sky are estimated to be (34 ± 4)° and (46 ± 5)° for the blue- and redshifted jet, respectively. We found that the jet is more inclined than the previous estimation of 21°. The representative 3D velocities of the blue- and redshifted jets that are calculated by averaging the 3D velocity of each knot are (98 ± 4) km s^{-1} and (78 ± 1) km s^{-1}, respectively. The newly derived inclination angles and 3D velocities of the jets allow us to refine the physical parameters of the jets. The refined values of the mass-loss rate and mechanical power of the

[1]Department of Astronomy, Kyoto University, Kitashirakawa-Oiwake-cho, Sakyo-ku, Kyoto, 606-8502, Japan; [2]National Astronomical Observatory of Japan, 2-21-1 Osawa, Mitaka, Tokyo 181-8588, Japan; [3]Department of Astronomical Science, The Graduate University for Advanced Studies, SOKENDAI, 2-21-1 Osawa, Mitaka, Tokyo 181-8588, Japan; [4]Academia Sinica Institute of Astronomy and Astrophysics, 11F of ASMA Building, No.1, Sec. 4, Roosevelt Rd, Taipei 10617, Taiwan; [5]Max-Planck-Institut für extraterrestrische Physik, Giessenbachstrasse 1, D-85748 Garching, Germany; 6Korea Astronomy and Space Science Institute (KASI), 776 Daedeokdae-ro, Yuseong-gu, Daejeon 34055, Republic of Korea

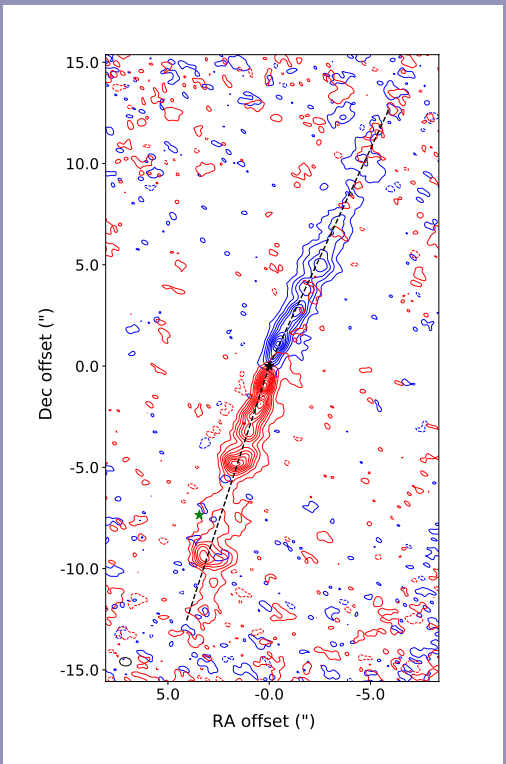

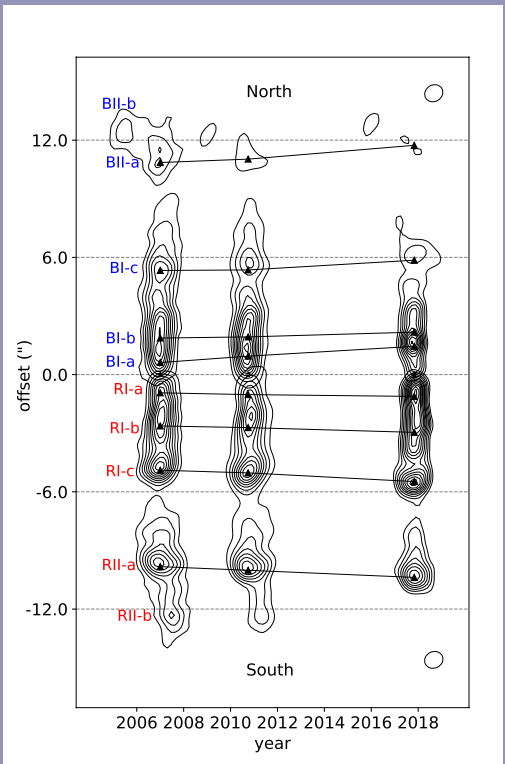

Figure 1 (left): High-velocity SiO emission. The velocity ranges are $\Delta V = \pm 41 - 70$ km s^{-1} with respect to the systemic velocity (v_{LSR} ~5 km s^{-1}). The contours start at 3σ and increase in 5σ intervals with 1σ = 0.23 Jy beam^{-1}. The black and green stars indicate the positions of the protostars, L1448C(N) and L1448C(S), respectively.

Figure 2 (right): The SiO moment 0 maps ($\Delta V = \pm 41 - 70$ km s^{-1}) in three epochs. The images of the blue- and redshifted jets were rotated so that the jet axes align with the vertical line. The triangles indicate the peak positions of each knot in PV diagrams.

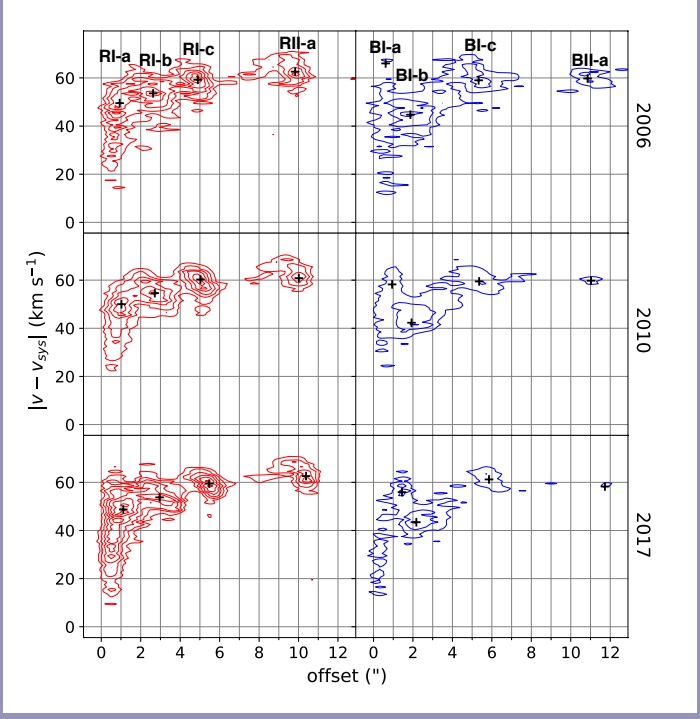

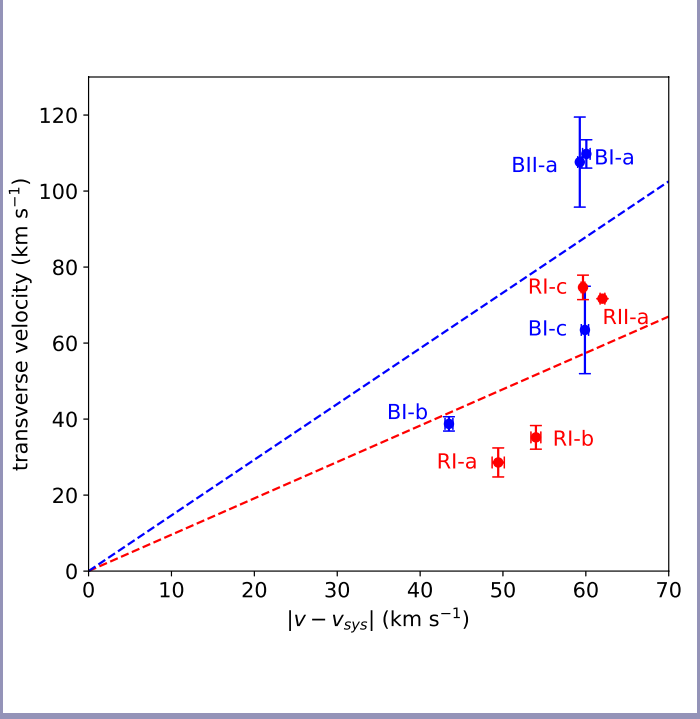

Figure 3: PV diagrams of the SiO jets in the 3 epochs. The positions of each knot are marked with black crosses.

Figure 4: Radial vs. transverse velocities of each knot. The dashed lines mean the fitted line for the knots on each side. The angles from the the plain of the sky (y-axis) are 34° for the blue line, and 46° for the red line.

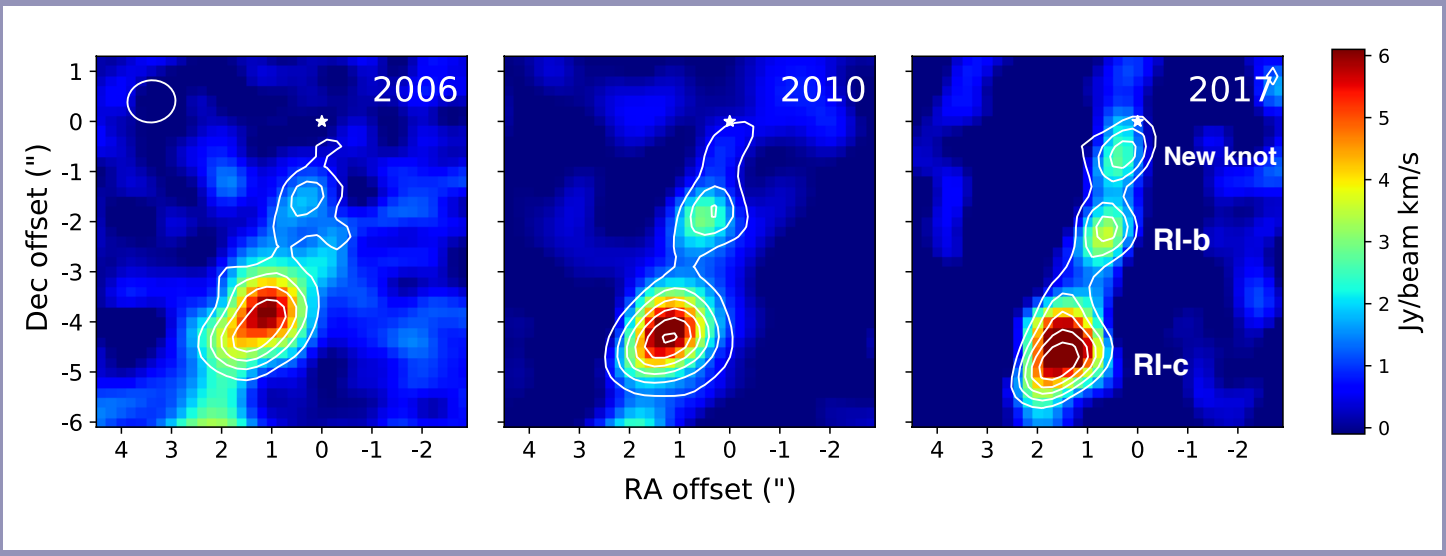

Figure 5: SiO (contours) and CO (color scale) moment zero maps in three epochs. Both the SiO and CO emission were integrated over ΔV ~61 – 70 km s^{-1}. White star indicates the central source.

both-sided jets are ~1.8 × 10^{-6} $M_\odot$ and ~1.3 $L_\odot$, respectively. The mechanical power of the jet is an order of magnitude lower than the bolometric luminosity; the L1448C(N) jet is no longer "extremely active".

One of the unexpected discoveries is a new ejection event; in the image of 2017, a newly appeared knot is detected for the first time at the base of the redshifted jet (Figure 5). The location of the new knot is ~0".77 (2230 au) away from the central star. If the 3D velocity of this new knot is same as the representative velocity of the redshifted jet, ~78 km s^{-1}, the dynamical timescale of the knot is estimated to be ~20 yr. Within this 20 yr, the averaged mass-loss rate of the new knot is estimated to be ~1.7 × 10^{-6} $M_\odot yr^{-1}$. This value is ~3 times higher than that of the whole redshifted jet, ~6.6 × 10^{-7} $M_\odot yr^{-1}$, implying a variability of mass-loss rate in the short timescale. In addition to the appearance of the new knot, the 345 GHz continuum flux of the centeral source has increased by ~37% between 2010 and 2017. Since the dynamical timescale of the new knot is ~20 yr, it is unlikely a direct causal relationship between the continuum enhancement and the new knot. However, the variation suggests that the mass accretion in L1448C(N) varies in a short timescale of ~10 – 20 yr.

We also found that the downstream SiO knot, RII-b has dimmed (see Figure 2). The peak brightness temperature of this knot was ~15 K in 2006, but it dropped to ~5 K in 2017. This dimming can be interpreted by an expansion of knot rather than the spatial filtering effect of the interferometer or chemical effect; during the expansion, the knot lost its energy with a decreasing volume density.

In conclusion, our high resolution observations of the L1448C(N) protostellar jets refined the inclination angle and the physical parameters. Moreover, we revealed the possible variability of the accretion rate and the jet knot in a short timescale. Further details of this work have been published in Yoshida et al. (2021).

REFERENCES

- Bachiller, R., Martin-Pintado, J., & Fuente, A. 1991, A&A, 243, L21
- Girart, J. M., & Acord, J. M. 2001, ApJL, 552, L63
- Hirano, N., Ho, P. P., Liu, S.-Y., et al. 2010, ApJ, 717, 58
- Lee, C.-F. 2020, A&A Rv, 28, 1
- Nisini, B., Codella, C., Giannini, T., et al. 2007, A&A, 462, 163
- Ortiz-Le´on, G. N., Loinard, L., Dzib, S. A., et al. 2018, ApJ, 865, 73
- Tobin, J. J., Looney, L. W., Mundy, L. G., Kwon, W., & Hamidouche, M. 2007, ApJ, 659, 1404
- Yoshida, T., Hsieh, T.-H., Hirano, N., & Aso, Y. 2021, ApJ, 906, 112

RESOLVED MEASUREMENTS OF GMCS IN M31: CO ISOTOPOLOGUES AND THE DUST

Charles J. Lada (CfA), Jan Forbrich (University of Hertfordshire, CfA), Sébastien Viaene (Universiteit Ghent), Glen Petitpas (CfA), and Chris Faesi (UMASS Amherst)

Giant molecular clouds (GMCs) are both fascinating and fundamental objects of astronomy. They are the primary sites of star and planet formation. Star formation drives the evolution of galaxies and in doing so the evolution of the cosmos itself. The attendant process of planet formation is a necessary condition for the development of life as we know it. GMCs are the at the nexus of these indispensable processes of nature. Deciphering the physical nature of GMCs is of paramount importance to achieve a basic and complete understanding of both star and planet formation and galaxy evolution.

Now, a half century since their discovery, many of the basic properties of GMCs have been well characterized in the Milky Way (e.g., Larson 1981, Solomon et al. 1987, Heyer & Dame 2015). In particular, GMCs in the greater solar neighbourhood have been probed in exquisite detail using observations of dust, both in emission and absorption and spectral lines from a variety of rare molecular species. Moreover, observations at infrared wavelengths from the ground and space have enabled comprehensive studies of young stellar objects and the star formation process in these very same GMCs. These studies provided detailed knowledge of the evolutionary stages of the formation of individual stars as well as robust measurements of the global star formation rates within individual GMCs. Together these measurements enabled the finding of a relatively tight correlation between the star formation rate, SFR, and the dense gas mass of the GMCs (Lada et al 2010; Lada et al. 2012) and demonstrated that, in contrast to global

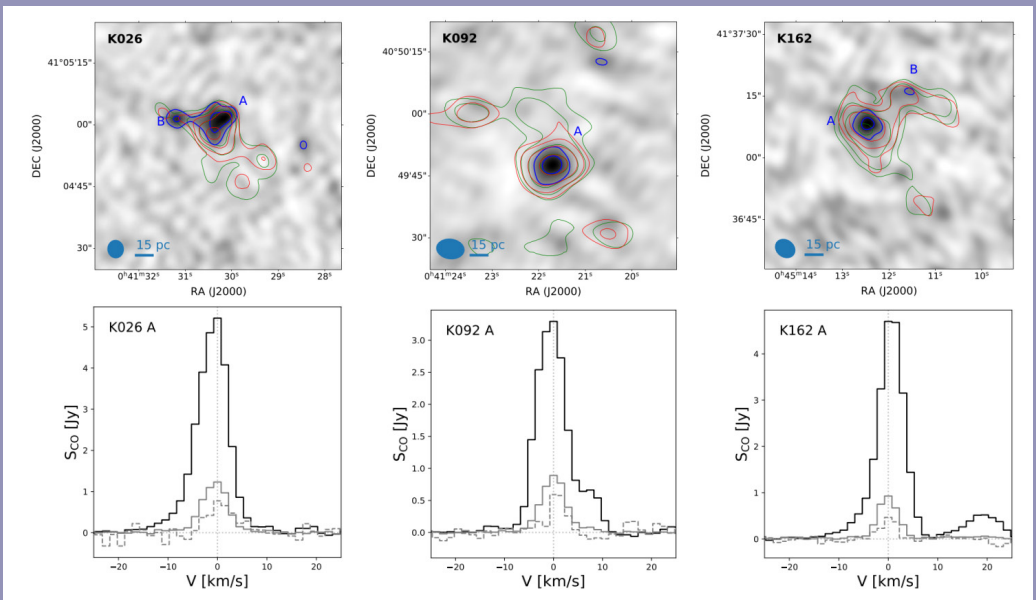

Figure 1: Examples of GMCs detected in the three CO isotopologues and in dust continuum emission from our SMA survey. **Top:** Contour maps of ^{12}CO (green), ^{13}CO(red) and continuum emission (blue) overlaid on a greyscale image of the 230 GHz continuum emission. Bottom: Corresponding spectra of ^{12}CO (black), ^{13}CO (grey) and C^{18}O (grey dashed). The C^{18}O spectrum has been multiplied by a factor 5 for clarity.

measurements of galaxies, the ensemble of individual GMCs in the Galaxy cannot obey a Kennicutt-Schmidt star formation law (Lada et al. 2013). But, it is not yet clear how representative these local GMCs (and the star formation process within them) are of GMCs in other galaxies or even in other parts of the Milky Way. Observations of external galaxies do suggest that broad similarities exist between local and extragalactic GMC populations (e.g., Bolatto et al. 2008). However, there is also evidence that variations of cloud properties exist between galaxies (e.g., Sun et al. 2018) and that under extreme environmental conditions the nature of molecular clouds and the star formation process within them can be strongly modified (e.g., Downes & Solomon 1998). Even in the Milky Way the GMCs that inhabit its very central regions do appear physically different from local GMCs (e.g., Longmore et al. 2013, Kruijssen et al. 2014). There are also hints of variations of GMC properties with position in the Galactic disk, but such variations are not sufficiently significant to be easily teased out of existing data due to our disadvantaged location observing from within the Milky Way galaxy (e.g., Lada & Dame 2020).

To better constrain differences between the physical properties of local GMCs and those in other galaxies it is necessary to obtain observations of extragalactic GMCs in a detail as close as possible to what can be achieved in the Milky Way. In particular, we want to be able to probe physical conditions in GMCs on sub-cloud spatial scales (i.e., ~10-15 pc). This requires both high sensitivity and spatial resolution observations of both gas and *dust* in these objects. Millimeter/submillimeter-wave interferometers provide the necessary spatial resolution to make such measurements in the closest galaxies. For some time such instruments have had sufficient sensitivity to detect and resolve CO emission from GMCs in the nearest galaxies (e.g., Vogel et al. 1987, Faesi et al. 2018, Leroy et al. 2021). But only very recently have improvements in receiver bandwidths provided the necessary continuum sensitivity to enable such interferometers to detect dust emission from individual GMCs in the nearest extragalactic systems. Most notably, the recent upgrade to wide-band continuum receivers on the SMA has provided the capability, for the first time, to obtain resolved measurements of dust emission in individual GMCs within the nearest spiral galaxy, M31, the Andromeda galaxy. This development motivated us to conduct the first dedicated survey for dust (continuum) emission on sub-GMC spatial scales in an external galaxy. Using the SMA we are presently in the process of obtaining a deep and simultaneous survey of broad band continuum and CO emission at 230 GHz of ~100 individual GMCs in M31. For these observations we use the subcompact configuration of the array. This configuration provides us with a perfect spatial match for mapping sub-cloud structure of individual GMCs in M31, delivering a maximum resolvable scale of ~100 pc with a resolution of ~15 pc. Our initial papers (Forbrich et al. 2020, Viaene et al. 2021) described the early results of the survey and reported the first resolved measurements of dust emission on sub-cloud spatial scales within the individual GMCs of a massive external galaxy.

Being able to measure dust emission on sub-GMC scales is significant. In the Milky Way such measurements are the 'gold standard' for determinations of basic GMC properties such as mass, size and structure (e.g., Lada et al. 2007, Goodman et al. 2009). This is because GMCs are composed almost entirely of molecular hydrogen (H_2) gas but since H_2 lacks a permanent dipole moment, GMCs are H_2 dark. Dust is the next most abundant constituent in GMCs and accounts for ~1% of their mass. Dust extinction and emission measurements are considered the most robust tracers of H_2 gas in GMCs. To date we have detected dust emission in 35 of 45 GMCs that we have mapped in M31. Combined with simultaneously observed ^{12}CO(2-1) emission we have been able to use the dust observations to derive GMC masses and directly measure α_{CO}, the mass-to-light ratio of CO, in individual M31 GMCs. The importance of the α_{CO} parameter lies in the fact that it is used to convert a CO detection to a total gas mass. Knowledge of α_{CO} is essential for molecular cloud mass measurements when dust cannot be independently observed. Unfortunately, this is still generally the case for extragalactic molecular clouds since dust emission from individual GMCs is so inherently weak and extremely difficult to detect in all but the nearest galaxies. Consequently measurements of α_{CO}, such as those we are obtaining for M31, are essential to help calibrate the use of this parameter for mass determinations of extragalactic GMCs.

Our most recent analysis of the M31 data yielded a value of α_{CO} = 8.7±3.9 $M_\odot$ (K km s^{-1} pc^2)$^{-1}$. for the J=2-1 transition of ^{12}CO from averaging the individual cloud determinations (Viaene et al. 2021). This is somewhat higher but consistent within the uncertainties with the Milky Way value (6.1) for the J=2-1 transition. Moreover, we note that the Milky Way value is itself uncertain by a factor of ~1.3 (Bolatto et al. 2013). However, it is presently unclear whether the extent to which the relatively large dispersion in the derived values of the α_{CO}(J=2-1) in M 31 is either intrinsic or due to observational error. Interestingly, we found no evidence for a variation of α_{CO}(J=2-1) with galactocentric radius in M31. Our measurements have been facilitated by the fact that the SMA enabled the CO and dust continuum data to be obtained simultaneously with identical observing conditions, calibration, spatial filtering, and astrometry.

Because the depth of our SMA observations was set by the requirement to acquire good signal-to-noise measurements of dust continuum emission in individual M31 GMCs, we also

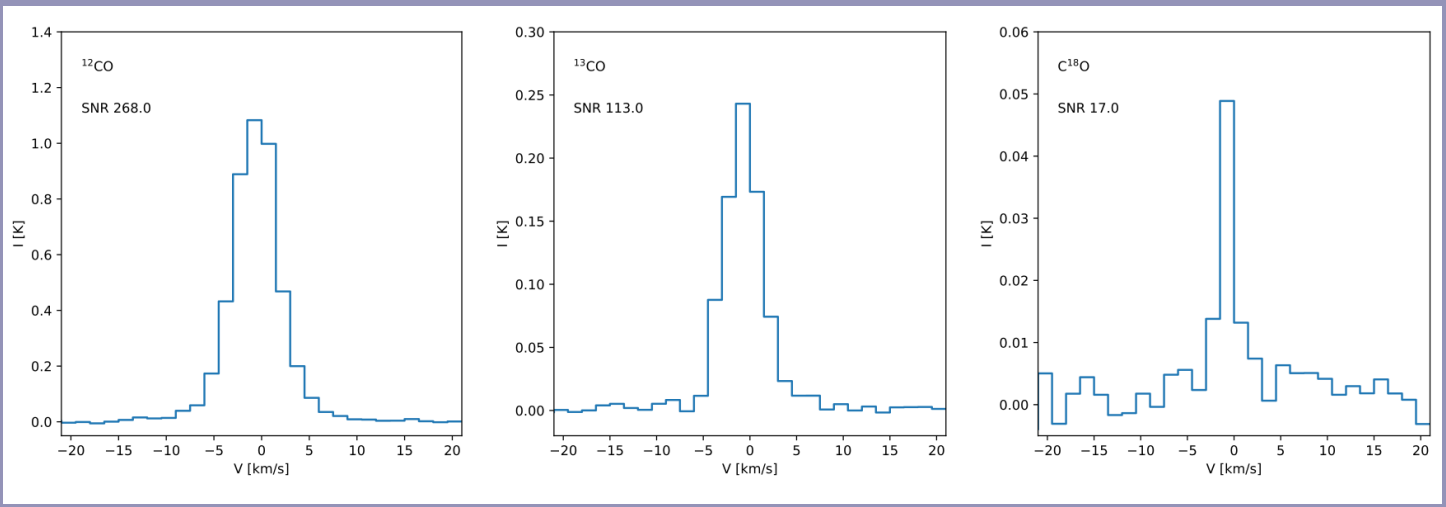

Figure 2: Median stacked (J=2-1) spectra of the three CO isotopologues for dust emitting clouds in M31. The resulting S/N is indicated in the top left of each panel.

simultaneously obtained exceptionally high signal-to-noise measurements of CO emission from its three primary, but rare, isotopologues, ^{12}CO, ^{13}CO and C^{18}O. Indeed, these SMA observations were sufficiently deep to enable us to trace the entire extent of ^{12}CO gas within the individual GMCs (Viaene et al. 2021) as was verified by simulations that will be discussed later in this article. As a result, we can make robust measurements of the full sizes of the GMCs we observe. As an additional measure of the remarkable depth of our observations, the ^{13}CO emission from the GMCs was found to be almost as extended as the ^{12}CO emission, typically encompassing 70% of the area of the ^{12}CO emission. Both these CO isotopologues were found to be more extended than the emission from the dust. This is to be expected as our simulations indicate that our sensitivity is a factor of ~2-3 lower than that needed to detect the dust emission over the full extents of these GMCs. Figure 1 shows maps of ^{12}CO and ^{13}CO emission superposed on maps of 230 GHz dust continuum emission in three of the GMCs in which emission from the rare C^{18}O isotopologue was also detected (but not spatially resolved). The spectra of all three CO lines are shown for each cloud as well. To our knowledge these are among the first detections of C^{18}O emission from individual GMCs in a massive external galaxy. Similar to the ^{12}CO observations we derived a ^{13}CO conversion factor of α_{13} = 48.9±20.4 from averaging over the individual GMC values. As of yet there is no generally accepted value of this parameter in the Milky Way and in terms of sample size and uniformity of data, our measurement of α_{13} in M31 is unique. Because ^{13}CO emission is considerably less opaque than ^{12}CO emission, this conversion factor may be ultimately more useful for estimating masses of molecular gas, not only in individual extragalactic GMCs, but also in globally averaged measurements of external galaxies.

We measured the integrated intensity ratios of ^{12}CO to ^{13}CO emission in the M31 GMCs to range from 4 -10 with a median value of 6.1, comparable to the range in values (5.5 -6.7) measured in the Milky Way using the 1-0 transition of CO (e.g. Solomon et al. 1979; Polk et al. 1988). Our results are also generally consistent with measurements in other nearby galaxies made at lower spatial resolution also using the 1-0 transition of CO (e.g., Schinnerer et al. 2010). We found the ratio we measured in M31 not to vary with galactocentric radius or with line intensity or dust surface density. We also measured the integrated intensity ratio of ^{13}CO to C^{18}O emission. This ratio ranges between 8 – 13 with a median value of 11 in our M31 cloud sample. This compares to the value of 7.9 derived from averaging over 9 nearby galaxy disks (Jimenez-Donaire et al. 2017).

Figure 2 shows the stacked spectra of the three CO isotopologues spatially integrated over 29 dust emitting areas (peaks) contained within 20 GMCs in M31. As can been seen the spectra are all characterized by high signal-to-noise. Combining these observations with our dust observations produced the first direct measurements of the abundances of these species in the individual GMCs of an external galaxy. Assuming optically thin emission and LTE we determined the following abundances (relative to H_2) for the two isotopologues: [^{13}CO] = 2.95 x 10^{-6} and [C^{18}O] = 0.44 x 10^{-6} with uncertainties of order 20% for both species (Viaene et al. 2021). The ^{13}CO abundance is in excellent agreement with that derived for Milky Way clouds (~2 x 10^{-6}; Dickman 1978, Frerking et al 1982, etc.) However, the C^{18}O abundance appears to be about a factor of 2 higher than that found in recent measurements of individual Milky Way clouds (e.g., Lewis et al. 2021, Roueff et al. 2020). Yet the isotopic abundance ratio we find (6.7±2.9) agrees within the uncertainties with the average Milky Way

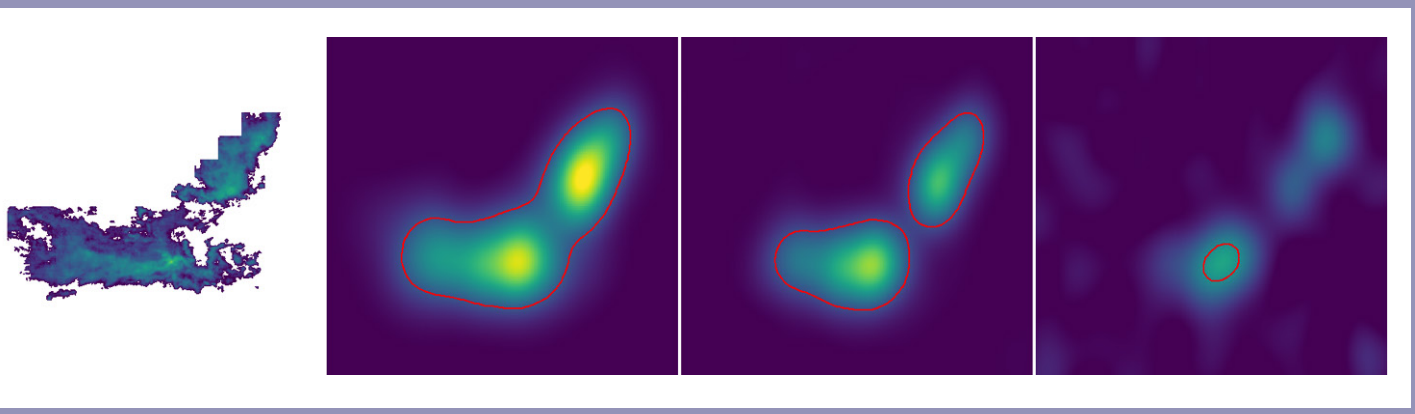

Figure 3: Results of simulations of the detectability of the famous Orion molecular clouds if at the distance of M31 and observed with the SMA in subcompact configuration. From left to right: original ^{12}CO image from Nishimura et al. 2015, simulated images of ^{12}CO emission, ^{13}CO emission and C^{18}O emission. Red contour indicates S/N ratios of 300, 30 and 3 for the ^{12}CO, ^{13}CO and C^{18}O simulated maps, respectively. These simulations show that our SMA observations are sufficiently sensitive to detect the entire spatial extent of ^{12}CO emission from an Orion-like GMC in M31. They predict that ~70% of the cloud's extent is detectable in ^{13}CO emission, similar to what is observed in our SMA survey of M31.

value (8.1, Wilson 1999). Using the stacked C^{18}O spectrum we can also determine the mass-to-light ratio for this very rare isotopologue. The value we derived from this exercise was found to be α_{18} = 345 (+25 -31). At the present time, the literature contains too few such measurements within the Milky Way and beyond to enable meaningful comparisons with M31. Here, as with ^{13}CO, our measurement of α_{18} is unique; this is the first time it has been derived at this spatial scale in an extragalactic source.

To place our observations in better context with what is observed in the Milky Way, we performed simulations to estimate how the local Orion GMCs would appear to the SMA if located in M31. We used the ^{12}CO, ^{13}CO and C^{18}O J=2-1 images of the Orion complex obtained by Nishimura et al. (2015) as the inputs for constructing the simulations. Figure 3 shows simulated integrated intensity images of the Orion GMC complex in the three CO isotopologues as they would appear in M31 if observed with the SMA in the subcompact configuration of the array. Also shown is the original ^{12}CO (J=2-1) image of the Orion complex obtained by Nishimura et al. (2015) for comparison. This exercise demonstrates that, if at the distance of M31, the Orion GMCs would be readily detected in our SMA survey. Indeed, our sensitivity is sufficient to detect the entire extent of the ^{12}CO gas in the Orion clouds at the distance of M31. That is, our data is completely capable of producing robust measurements of the full extents of individual GMCs in M31. The simulations also indicate that ^{13}CO emission should be readily detected over a significant portion of a GMC in M31. In the simulated images the ratio of the surface areas of ^{13}CO to ^{12}CO emission (above the corresponding S/N = 3 contours) is 72%. As mentioned earlier this is close to what we observe for the M31 GMCs in our SMA current sample. Finally the simulations suggest that C^{18}O would be detectable in an Orion like cloud in M31, but even deeper observations would be required to detect extended emission from this rare isotopologue. Again, this is entirely consistent with what we have observed in the M31 GMCs. Similar simulations were performed using Planck 230 GHz continuum maps of Orion as input to evaluate the detectability of dust emission in M31 clouds. These simulations indicate that we likely detect only 20-30% of the full extent of the cloud's dust emission at 230 GHz with our current sensitivity, consistent with what is found comparing the extents of continuum and CO emission in the current survey data. Remarkably these simulations also suggest that once the full 64 GHz bandwidth capability is deployed on the SMA receivers, the entire extent of an M31 GMC can be detected in dust continuum emission with only two full tracks of integration.

At the mid-point of our survey of the GMC population in M31 our preliminary results indicate that a number of the fundamental properties of these objects span a similar range to those of GMCs in the local Milky Way. This supports results suggested by even some of the earliest observations of CO (and HI) on cloud scales in M31 (Vogel et al. 1987, Lada et al 1988, Rosolowsky 2007). Moreover, now our overall knowledge of these objects has been greatly enhanced with the first resolved measurements of dust emission in this extragalactic GMC population. Our knowledge of the GMCs in M31 should improve even further with the larger sample of clouds that will be produced at the conclusion of the survey and with more detailed analysis, particularly when the velocity information in the CO data is included. The latter analysis will provide valuable additional information leading to more complete and accurate cloud identifications and to direct

investigation of the dynamical properties of these objects. This, in turn, will enable us to investigate other fundamental properties of the GMC population, such as the Larson scaling relations, in a detail very close to that obtained for local Milky Way GMCs. Finally, looking toward the near future, we will be able to investigate the star formation law for the GMC population in M31 by measuring star formation rates on sub-cloud scales using a centimetric continuum survey of the galaxy we have obtained with the VLA and an optical emission-line survey of HII regions associated with the M31 GMCs we recently obtained with the MMT. Together these surveys are providing us with unparalleled measurements of the sub-cloud physical conditions and processes within the GMCs of the Andromeda galaxy. These are the first such systematic observations obtained for a large disk galaxy beyond the Milky Way and they are bringing us closer to our ultimate goal: to determine the physical nature of extragalactic GMCs and the star formation within them to a degree of precision roughly comparable to that obtained for the GMC population in the Milky Way.

REFERENCES

- Bolatto et al. 2008, 686, 948
- Bolatto et al. 2013, ARAA, 51, 207.
- Dickman, 1978, ApJS, 37, 407
- Forbrich et al. 2020, ApJ 890, 42
- Frerking et al. 1982, ApJ, 262, 590
- Goodman et al. 2009, ApJ 692, 91
- Faesi et al. 2018, ApJ 857, 19
- Heyer & Dame 2015, ARAA 53, 583
- Jimenez-Donaire et al. 2017, ApJL 836, L29
- Kirk et al. 2015, ApJ 798, 58
- Kruijssen et al. 2014, MNRAS 440, 3370
- Lada et al. 1988, ApJ 328, 143
- Lada et al. 2007, Protostars & Planets V, 3.
- Lada et al. 2012, ApJ 745, 190
- Lada et al. 2013, ApJ 778, 133
- Lada & Dame 2020, ApJ 898, 3
- Larson, 1981 MNRAS, 194 809
- Leroy et al. 2021, ApJS, in press.
- Lewis et al. 2021 ApJ, 908, 76
- Longmore, 2013, MNRAS 429,9 87
- Lombardi et al. 2010, A&A 519, L7
- Lombardi et al. 2014 , A&A 566, 45
- Madau & Dickinson 2014, ARA&A 52, 145
- Polk et al. 1988, ApJ 332, 432
- Rosolowsky, E. 2007, ApJ, 654, 240
- Roueff et al. 2020, A&A, 645, A26
- Schinnerer et al. 2010, ApJ 719, 1588
- Solomon et al. 1979, ApJ 232, 89
- Solomon et al. 1987, ApJ 319, 730
- Sun et al. 2018 ApJ 860, 172
- Viaene et al. 2021, ApJ, 912, 68
- Vogel et al. 1987, ApJL 321, 125
- Wilson, 1999 RPPh, 62, 143

THE NATURE OF 500 MICRON RISERS I: SMA OBSERVATIONS

J. Greenslade[1], D.L. Clements[1], G. Petitpas[2], V. Asboth[3], A. Conley[4], I. Pérez-Fournon[5,6], D. Riechers[7,8,9]

The role and nature of dusty star forming galaxies (DSFGs) at high redshifts (z > 4) is currently unclear. Observations with *Herschel* have identified an unexpectedly large population of candidate high-z DSFGs through color selection in the three bands of its SPIRE instrument (e.g., Dowell et al. 2014). This selection is based on finding a rising spectral energy distribution (SED) from 250 to 500 μm, leading to these sources being termed '500-risers'. Since the far-IR SED of a typical galaxy peaks at around 100 μm in the rest frame, sources whose SED is still rising at 500 μm are likely to lie at z > 4. Such sources, if at z > 4, would have luminosities > 10^{13} L_{sun} and star formation rates >1000 M_{sun}/yr. They would thus be extreme objects and as such could represent the high luminosity end of a larger population of DSFGs at high redshift (see e.g. Greenslade et al., 2019).

However, spectroscopic redshifts have been obtained for only a tiny fraction of this population and so its properties are only weakly constrained, and there is disagreement on whether this population contributes significantly to the cosmic SFR-density (SFRD) above z > 4. It has even been suggested that current data are unable to tell the difference between models where high-z DSFGs dominate the SFRD or not (Casey et al. 2018). The nature of the individual 500-risers that make up this population is also in dispute. Simulations suggest that most of the fainter 500 μm risers are unresolved galaxy blends, whereas the brighter ones (S500 > 60 mJy)

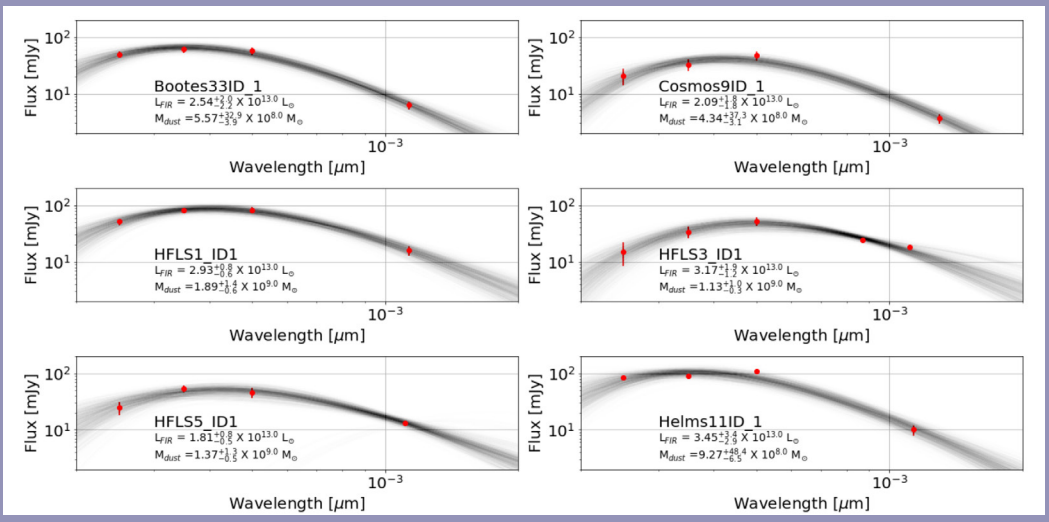

Figure 1: Sampled SED fits to the SPIRE and SMA flux densities measured for sources where we only detect a single counterpart to the SPIRE source. The black lines show 1,000 samples after fitting, while the red points give the flux densities and error bars to the observed photometry of each source. Names, estimated FIR luminosities and estimated dust masses are provided as text on each of the plots.

[1] Imperial College London, Prince Consort Road, London SW7 2AZ, UK; [2] Harvard-Smithsonian Center for Astrophysics, 60 Garden Street, Cambridge, MA 02138; [3] Department of Physics and Astronomy, University of British Columbia, 6224 Agricultural Road, Vancouver, BC V6T-1Z1, Canada; [4] Center for Astrophysics and Space Astronomy 389-UCB, University of Colorado, Boulder, CO, 80309, USA; [5] Instituto de Astrofísica de Canarias, C/ Vía Láctea, E-38200 La Laguna, Tenerife, Spain; [6] Departimento de Astrofísica, Universidad de La Laguna, E-38206, La Laguna, Tenerife, Spain; [7] Cornell University, 220 Space Sciences Building, Ithaca, NY 14853, USA; [8] Max-Planck-Institut für Astronomie, Königstuhl 17, D-69117 Heidelberg, Germany

are almost all single gravitationally lensed galaxies (Béthermin et al 2017).

The ideal test of the nature of the 500-riser population is to conduct submm interferomteric observations with resolutions of a few arcseconds or better. This will be able to determine the multiplicity fraction and, at higher resolutions, examine the role of gravitational lensing. We present here Submillimeter Array (SMA; Ho et al. 2004) observations of 34 500-risers to determine the multiplicity of these sources. Our targets were observed over the period from 2010 May 19 to 2015 May 7. The observations were made at a variety of different tunings but generally at frequencies close to either 345 or 265 GHz. The most common configuration used was Compact but observations of specific sources in Subcompact, Extended and, in two cases, Very Extended were also used. A mixture of full tracks, partial tracks and track sharing was used for these observations, resulting in different sampling of the uv plane. Each of the data sets was calibrated using standard procedures within the IDL package MIR and the data were then exported to the analysis package MIRIAD (Sault et al. 2011) for further reduction. We used the MIRIAD command *invert* to transform the visibilities into (dirty) maps, choosing a natural weighting (i.e. constant weight to all visibilities) since this maximizes the signal to noise of any sources present. We then CLEANed our maps, using 250 CLEAN iterations. The noise level varies between maps, but on the CLEANed maps was typically around 1.5 - 0.5 mJy, with minimum and maximum values of 0.5 mJy and 2.9 mJy respectively. We extract sources and fluxes from the dirty maps rather than the CLEANed maps and for the dirty maps our noise values had a mean of 2.2 +/- 0.9 mJy, with minimum and maximum values of 0.8 mJy and 4.9 mJy respectively. Experiments were performed using different weighting schemes and cleaning parameters, using both the data and simulations and we found that the process described above generally performed best at recovering the flux density of injected fake sources.

We detect 26 sources associated with our 34 *Herschel* selected 500-risers. Three of these sources are detected at two different frequencies in the SMA maps. Of our 34 500-risers, 12 (35%) have no detections with the SMA, 18 (53%) have a single detection, and 4 (12%) have two detections, indicating that at these flux density limits and resolutions, most 500 μm risers appear to be single sources. Of the 17 SPIRE sources with S500 > 60 mJy, which Béthermin et al. (2017) predict to be almost entirely single sources, we find 12 that appear to be single sources, 3 have multiple detections, and 2 have zero detections. One of the multiple sources, Lock2, has one counterpart at 345 GHz but two at 270 GHz. Curiously, the source detected at both 345 GHz and 270 GHz is the fainter of the two sources at 270 GHz, with only 5.68 +/- 0.94 mJy at 270 GHz compared to the other source which has a flux of 9.07 +/- 0.94 mJy but no counterpart at 345 GHz. The maps where we detect no sources are likely to be made up of multiple faint sources below the detection limit. This means that of our 17 SPIRE sources with S500 > 60 mJy, 5 (30%) are multiple galaxies. Such a high fraction would appear to disagree with Béthermin et al. (2017), who suggest such sources are almost entirely lensed single sources. We can only say with certainty that the maps where we detect 2 sources are definitely multiples; in maps where we detect a single source, there may be a secondary fainter source, and in maps where we detect no sources, we can at best put upper limits to any detection.

The Physical Properties of 500-risers

To determine the physical parameters of our single sources, we take the measured SPIRE and SMA flux densities, and, following literature convention fit them to a single temperature modified blackbody function assuming the spectral index to be ~1.5 - 2 for SMGs (Blain 2002; Casey et al. 2014). We use the affine invariant Markov Chain Monte Carlo (Goodman & Weare 2010) ensamble sampler Python package *emcee* (Foreman-Mackey et al. 2013) to fit this model to our data. A sample of the fits is shown in Figure 1. We find that sources where we detect a single SMA counterpart all have luminosities > 10^{13} M_{sun}, leading to their classification as Hyper-Luminous Infrared Galaxies (HLIRGs). While lensing may have boosted the derived luminosity of some sources, a modest lensing amplification at the level of 2 - 3, as is the case for HFLS3 (Cooray et al. 2014) would still leave most of our sources as HLIRGs. In the absence of any AGN contribution to their high far-IR luminosity, the derived SFR for these objects is in excess of 1000 M_{sun}/yr, with some sources potentially having SFRs in excess of 5000 M_{sun} /yr, leading to their classification as Extreme Starbursts (Rowan-Robinson et al. 2018), a class of object that cannot be accounted for by any current model of galaxy formation. The simulations used by Béthermin et al. (2017) to determine the effects of source clustering on single dish instruments limited the maximal starburst to 1000 M_{sun} /yr. We here show that sources beyond this limit exist in the 500-riser population, so it is likely that the results of the clustering simulations are in need of revision at the brightest fluxes. Further observations at complementary wavelengths, including the optical, X-ray and far-IR spectroscopy, will be needed to determine what role AGNs play in powering these sources.

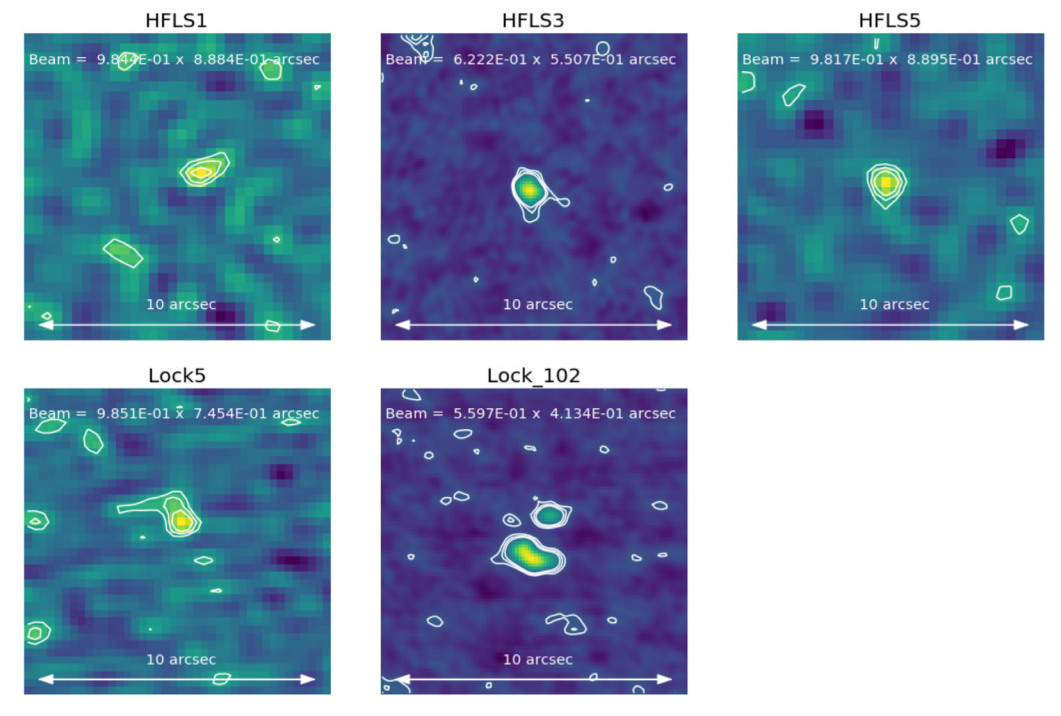

Figure 2: Extended (all maps) and very extended (HFLS3 and Lock_102) only) observations on maps where these configurations are available. All maps are 10 arcsec x 10 arcsec, and orientated so that north is up and east is to the left. Contours show 2, 3, 4 and 5 sigma levels. The beam is approximated as a Gaussian, with semi-major and semi-minor axis given in the text at the top of each image.

The Role of Lensing

One of our sources is known to be strongly lensed (Lock_102), and another (HFLS3) is weakly lensed with a magnification of 1.3 (Riechers et al. 2013). Seventeen of our sources have S500 > 60 mJy, which Béthermin et al. (2017) suggest should all be lensed galaxies. However, we only have extended array observations for 5 of our sources (HFLS1, HFLS3, HFLS5, Lock5 and Lock_102), and the 2 – 4" beamsize in the compact and subcompact configurations lack the resolution necessary to provide a definitive test of lensing. In Figure 2, we show those sources where we do have extended or very extended configuration observations. The synthesized beams for these range from 1 to 0.35" across. Only one of these sources, Lock_102, clearly shows the arc-like structure indicating strong lensing, which is confirmed by observations at other telescopes. The other known lens, HFLS3 with a magnification ~ 2.2 +/- 0.3 (Cooray et al. 2014), appears reasonably compact, with some sign of extension to the north, but no obvious indications of lensing. Similar suggestions of extension are seen in HFLS1 and Lock5 whilst HFLS5 appears compact, indicating a diameter < 6.9 kpc. Both the current work and Oteo et al. (2017) find that the lensing fraction for 500-risers with flux densities > 60 mJy seems to be much lower than predicted by Béthermin et al. (2017).

The Role of Blended Sources

Béthermin et al. (2017) suggest that on average 60% of the flux of a S500 < 60 mJy Herschel source at 500 μm comes from a single object, while sources brighter than 60 mJy should largely be strongly lensed single sources. Our observations show a more complicated picture. Of the 17 sources in our sample with S500 > 60 mJy, three are found to have two counterparts and three are found to have no counterparts at all, suggesting that they are blends of three or more sources. This means that 35% of the sources in our sample with flux densities >60 mJy at 500 μm do not match the expectation that they should be single, strongly lensed sources. Instead they are blends of multiple components. At brighter fluxes, S500 > 100 mJy, they do appear to be single sources, with one, Lock_102, being a confirmed lens. At somewhat fainter fluxes, where lensing is still expected to dominate, we have counter-examples such as Bootes13, which resolves into 2 sources (S500 = 82 mJy) and Bootes15, where we detect no counterparts despite a flux density of S500 = 66 mJy. At fainter fluxes, S500 < 60 mJy, where 40% of sources are expected to be multiple, we find that of 17 sources, seven are single sources, is resolved into two components, and nine have no detection, suggesting that they are made up of multiple components, indicating a multiplicity fraction of 60%. In Figure 3, we plot a histogram of the 500 μm flux density of our sources split by whether we do or do not detect counterparts in our SMA maps. The maps where we do not detect any sources are generally fainter at 500 μm. This tends to support the conclusion of Béthermin et al. (2017) that sources below 60 mJy are more likely to be blends. However, with a likely multiplicity fraction of 60% our data suggest that the blended fraction is likely to be higher than the predicted 40%.

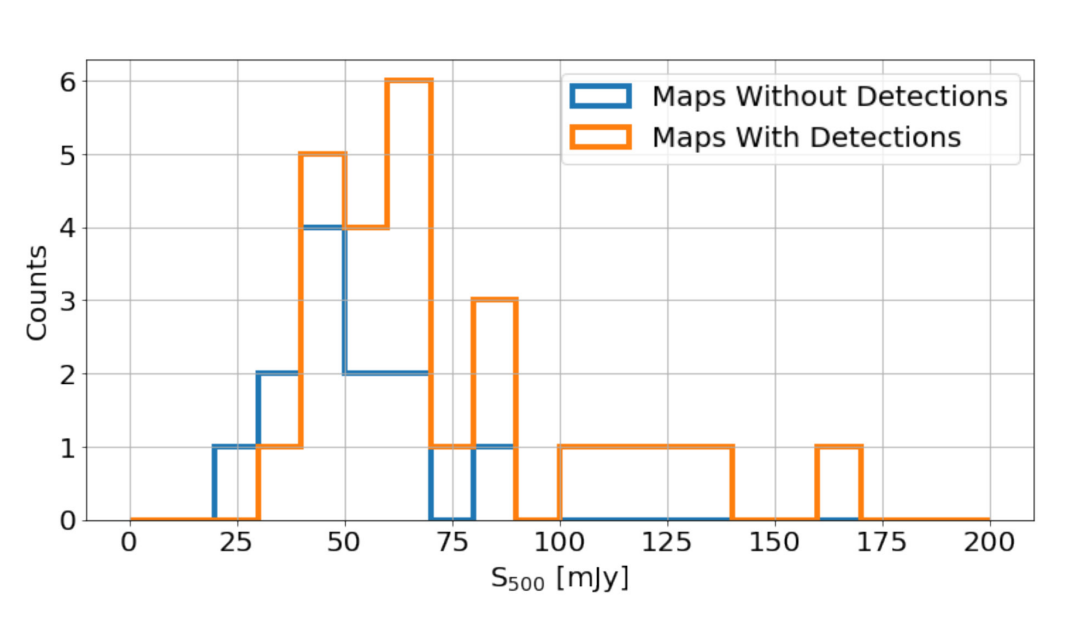

Figure 3: The Herschel 500 μm flux density of a source, as a function of whether a source is detected in the SMA map (orange histogram) or not (blue histogram). Bins are of width 20 mJy.

In conclusion, the 500-riser population seems likely to represent galaxies undergoing major bursts of star formation at very high redshifts. Such high luminosity objects were not considered in the Béthermin et al. (2017) models. Determining the broader role of this population in galaxy formation, and whether, as is likely for any reasonable luminosity function, there is an underlying much larger population of lower luminosity high redshift DSFGs, remain important tasks for far-IR and submm astronomy.

REFERENCES

- Bolatto et al. 2008, 686, 948
- Bolatto et al. 2013, ARAA, 51, 207.
- Dickman, 1978, ApJS, 37, 407
- Forbrich et al. 2020, ApJ 890, 42
- Frerking et al. 1982, ApJ, 262, 590
- Goodman et al. 2009, ApJ 692, 91
- Faesi et al. 2018, ApJ 857, 19
- Heyer & Dame 2015, ARAA 53, 583
- Jimenez-Donaire et al. 2017, ApJL 836, L29
- Kirk et al. 2015, ApJ 798, 58
- Kruijssen et al. 2014, MNRAS 440, 3370
- Lada et al. 1988, ApJ 328, 143
- Lada et al. 2007, Protostars & Planets V, 3.
- Lada et al. 2012, ApJ 745, 190
- Lada et al. 2013, ApJ 778, 133
- Lada & Dame 2020, ApJ 898, 3
- Larson, 1981 MNRAS, 194 809
- Leroy et al. 2021, ApJS, in press.
- Lewis et al. 2021 ApJ, 908, 76
- Longmore, 2013, MNRAS 429,9 87
- Lombardi et al. 2010, A&A 519, L7
- Lombardi et al. 2014 , A&A 566, 45
- Madau & Dickinson 2014, ARA&A 52, 145
- Polk et al. 1988, ApJ 332, 432
- Rosolowsky, E. 2007, ApJ, 654, 240
- Roueff et al. 2020, A&A, 645, A26
- Schinnerer et al. 2010, ApJ 719, 1588
- Solomon et al. 1979, ApJ 232, 89
- Solomon et al. 1987, ApJ 319, 730
- Sun et al. 2018 ApJ 860, 172
- Viaene et al. 2021, ApJ, 912, 68
- Vogel et al. 1987, ApJL 321, 125
- Wilson, 1999 RPPh, 62, 143

DEVELOPMENT OF A SILICON-CHIP-BASED WAVEGUIDE DIRECTIONAL COUPLER FOR THE WSMA

Lingzhen Zeng[1] , Wei-Chun Lu[2] , Paul K. Grimes[1], Tse-Jun Chen[2], Yen-Pin Chang[2], C. Edward Tong[1], and Ming-Jye Wang[2]

Background

A waveguide directional coupler can be used to inject a certain amount of the electromagnetic power propagating in a given direction from one waveguide to another, while isolating the power propagating in the reverse direction. This feature makes the directional couplers ideal for the local oscillator (LO) injection applications in the Superconductor - Insulator - Superconductor (SIS) receiver system. In the present SMA receiver system, LO power is injected via a room temperature optical beam splitter. For the new wSMA receiver system, one of the key upgrades is to perform the LO injection right in front of the SIS mixer using a waveguide directional coupler. By doing so, the sensitivity of the receivers will be expected to improve.

Fig.1 gives the functional block diagram of the wSMA receiver frontend. Before passing the sky signals to the SIS mixers, an orthogonal mode transducer (OMT) first separates the two linearly polarized components of the sky signal. Two couplers are then used, one for each polarization, to inject LO power independently into the pair of SIS mixers.

Over the past few decades, driven by applications in radio-astronomy and other fields, more and more standard waveguide components, including couplers, quadrature hybrids, OMTs and waveguide twist, are integrated into multi-function waveguide blocks operating in the millimeter wave to terahertz regime. In order to facilitate such integration, an easily machinable E-plane split block design is highly desired for the wSMA. We have designed a frontend module that integrates the OMT, coupler and associated waveguide twist. Here, we report the design of a new coupler design that lends readily to tight integration with the other components.

Traditional waveguide directional coupler design is not well adaptable to the machinable split-block geometry, especially

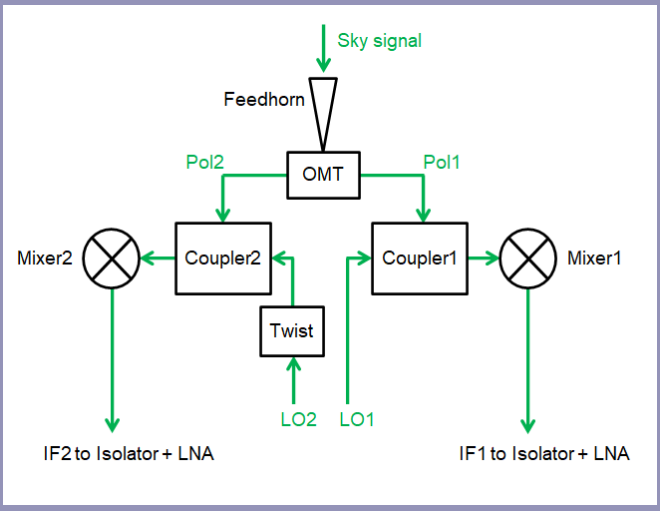

Figure 1: wSMA receiver frontend diagram.

[1] Center for Astrophysics | Harvard & Smithsonian, Cambridge, MA, USA;
[2] Institute of Astronomy & Astrophysics, Academia Sinica, Taipei, Taiwan

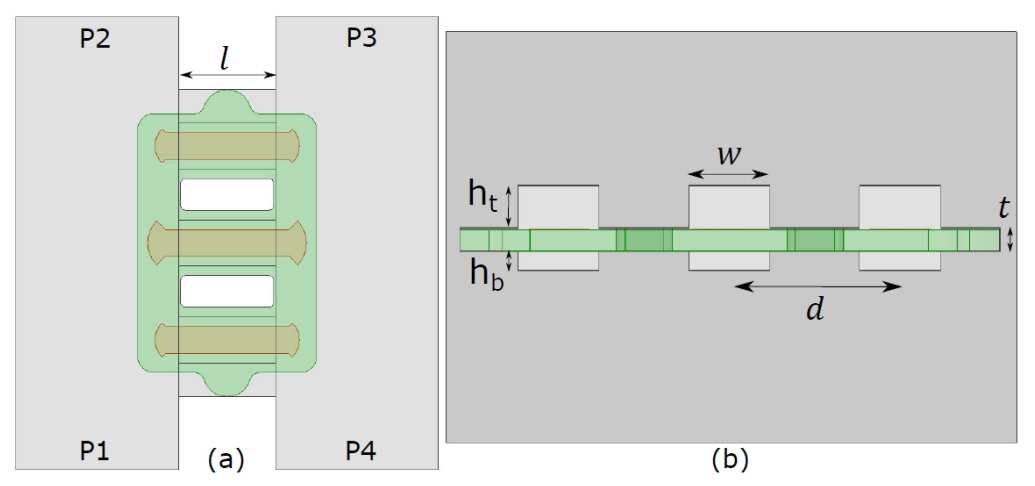

Figure 2: The CAD model of our coupler design. Panel (a) shows the top view and panel (b) shows the side view of the coupling section. Silicon substrate is shown in green color.

when weak couplings (< -10 dB) are needed, because these couplers require small size features for the weak coupling driving high fabrication tolerance. The direct machining design reported in [1] had high insertion loss and low isolation performance. The straight waveguide couplers [2, 3] and cross-guide couplers [4–6] required complicated coupling patterns with high tolerance requirements. They are of little use in split-block integrated waveguide circuits. The micro-machined design from [7, 8] reported an insertion loss of about 4 dB and an isolation only about 20 dB level from 330 GHz to 470 GHz. Split-block waveguide designs with multiple E-field coupling probes suspended on quartz substrates were proposed in [9–12]. Theoretically, these designs can offer couplings from -10 dB to -30 dB with isolation better than 30 dB. However, at frequencies above 200 GHz, the dimensions of the chips become very small, and it becomes exceedingly difficult to install and align each coupling chip in position. Actual measurement results could be very different compared to simulations [12].

Working together with ASIAA, the SMA receiver lab developed a novel machinable coupler design that offers a weak coupling of -18 ± 2 dB, with an isolation better than 30 dB over a 30% fractional bandwidth. Our design integrates multiple suspended stripline probes into a single silicon chip, which allows for easy chip installation and alignment. The measurement data of our prototypes agree well with our simulations.

Coupler Design and Optimization

As shown in Fig. 2, our coupler chip design consists of three pairs of suspended bow-tie coupling probes with two open slots in the center and two "ears" on the top and the bottom. The open slots are used to register the chip position in the block and eliminate any cross talks between adjacent probes. The ears are designed to provide better mechanical stability to the chip and for better chip handling during chip installation. In spite of its high dielectric constant, silicon substrate is used because the silicon chip fabrication process is well established, and the silicon chips are quite strong. In principle, we can achieve higher directivity by increasing the number of coupling probes. The three-probe design, however, already provides sufficient isolation for our front-end application.

Our coupler was simulated using the ANSYS Electronics Desktop Software Suite (a.k.a. HFSS). The initial design of the coupler was generated by calculating the coupling between waveguides for a single stripline probe coupler section with varying probe ra-

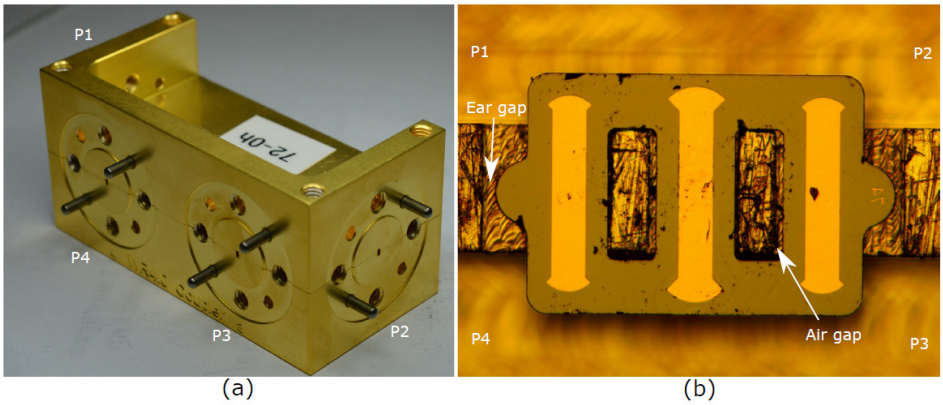

Figure 3: Photos of prototype WR4.0 coupler block (a) and a coupling chip installed in the block (b). The 4 waveguide ports are labelled as: P1 - input port, P2 - output port, P3 - coupled port, and P4 - isolation port.

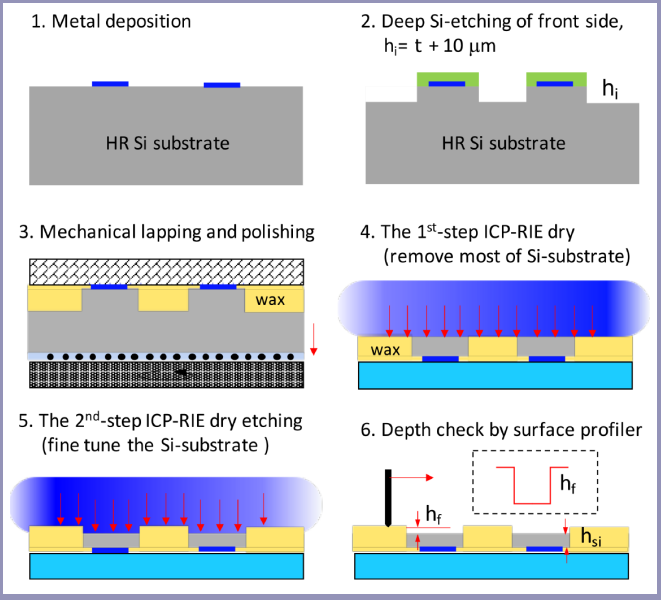

Figure 4: Coupler chip fabrication process. Steps 1 to 2 show the front-side deposition process. Steps 3 to 6 show the substrate thinning process from the back side.

dius, using a parametric sweep in HFSS. The radii of the probes on the three coupler sections were then selected to give the individual coupling constants required for a binomial response coupler design with the desired overall coupling [13]. This design method necessarily ignores the influence of the silicon substrate joining the individual coupler sections, and thus further optimization within HFSS is required once the initial design has been generated.

Coupler Fabrication and Measurement

Fig. 3 shows the photo of one of our prototype coupler blocks and that of a silicon chip installed in the block. The coupler is an E-plane split-block design with standard UG-387 waveguide ports. The main waveguide from the port P1 to P2 is a 50 mm long straight section, and a secondary waveguide in a "U" shape connection between the ports P3 and P4 forms the coupled waveguide. To facilitate chip installation, gaps around the chip slots are introduced between the chips and blocks.

The chip fabrication process, conducted in the clean room of ASIAA, consists of two major procedures: a front-side process followed by a substrate thinning process. The major steps are illustrated in Fig. 4. During the front-side process, a gold layer was deposited on a high resistance silicon substrate using an E-beam evaporator. The metalization pattern was defined by a lift-off process. Then, the geometry of the silicon chip was defined by a deep-silicon etching process with an over-etch depth of about 10 µm to ensure the accuracy of dimensions. After that, the substrate was flipped mounted on a carrier substrate. The substrate thinning process started with backside mechanical lapping/polishing to a thickness of about 100 µm. The substrate thickness was further reduced by inductively coupled plasma - reactive ion etching (ICP-RIE). Once the target thickness was achieved, the chips were separated on dismounting from the carrier substrate. The final thickness as measured by optical microscope, demonstrates that the final chip thickness was accurate to 2 µm.

The fabricated chips are very rigid and are easily mounted in the coupler block using vacuum tweezers. We fabricated four prototype blocks and many coupling chips with a matrix of different dimensions. The measurement results are highly consistent using different blocks. The S-parameter measurement results are plotted in Fig. 5. A comparison of the simulated coupling co-

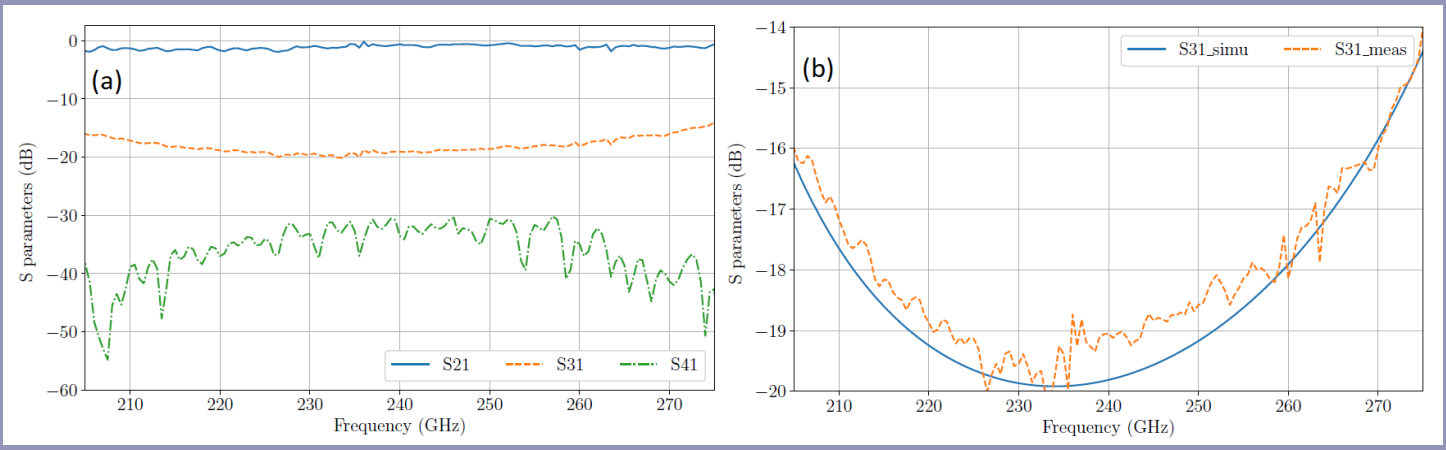

Figure 5: Panel (a) shows the WR4.0 coupler prototype measurement results. Panel (b) shows the simulated and measured S31 data.

efficient with the measured data is shown in Fig. 5 (b), demonstrating a very good agreement between simulated and experiment. The average insertion loss is about -1.25 dB across the band, which is consistent with that of a 50 mm long waveguide at room temperature. The isolation is better than 30 dB across the band, corresponding to a directivity of better than 12 dB in midband.

Future Development

Our coupler has been tested as an individual component. Recently, the coupler has been tested with the wSMA low band mixer in a lab cryostat. The results confirm that the coupler improves the sensitivity of the mixer. The next step is to measure the frontend assembly as a LO injection receiver system, in which the couplers play important roles.

REFERENCES

- S. M. Lewis, E. A. Nanni, and R. J. Temkin, "Direct machining of low-loss THz waveguide components with an RF choke," IEEE Microwave and Wireless ComponentsLetters, vol. 24, no. 12, pp. 842–844, 2014.
- H. Oraizi, "Optimum design of multihole directional couplers with arbitrary aperture spacing," IEEE Transactions on Microwave Theory and Techniques, vol. 46, no. 4, pp. 331–342, 1998.
- H. Ghorbaninejad and R. Heydarian, "New design of waveguide directional coupler using genetic algorithm," IEEE Microwave and Wireless Components Letters, vol. 26, no. 2, pp. 86–88, 2016.
- P. Meyer and J. C. Kruger, "Wideband crossed-guide waveguide directional couplers," in 1998 IEEE MTTS International Microwave Symposium Digest (Cat. No. 98CH36192), vol. 1, 1998, pp. 253–256 vol.1.
- J. A. R. Ball and T. M. Sulda, "Small aperture crossed waveguide broad-wall directional couplers," IEE Proceedings - Microwaves, Antennas and Propagation, vol. 147, no. 4, pp. 249–254, 2000.
- Y. Zhang, Q. Wang, and J. Ding, "A cross-guide waveguide directional coupler with high directivity and broad bandwidth," IEEE Microwave and Wireless Components Letters, vol. 23, no. 11, pp. 581–583, 2013.
- J. Hesler and A. Lichtenberger, "THz waveguide couplers using quartz micromachining," in 21st International Symposium on Space Terahertz Technology, Mar. 2010.
- J. T. Do, Q. Yu, J. L. Hesler, and N. S. Barker, "A 330-500 GHz micromachined directional coupler," in 2013 IEEE MTT-S International Microwave Symposium Digest (MTT), 2013, pp. 1–3.
- A. R. Kerr and N. Horner, "A split-block waveguide directional coupler," in Nat. Radio Astron. Observatory, Charlottesville, VA, USA, ALMA Memo #432, 2002.
- R. Monje, V. Belitsky, and V. Vassilev, "A novel design of broadband waveguide directional couplers and 3-db hybrids," in 2006 IEEE MTT-S International Microwave Symposium Digest, 2006, pp. 1169–1172.
- P. K. Grimes, M. J. R. Brock, C. M. Holler, J. John, M. E. Jones, O. G. King, J. Leech, A. C. Taylor, G. Yassin, K. Jacobs, and C. Groppi, "GUBBINS: A novel millimeter-wave heterodyne interferometer," in 20th International Symposium on Space Terahertz Technology, Apr. 2009.
- J. Leech, G. Yassin, B. Tan, Y. Zhou, J. Garrett, and P. Grimes, "An SIS mixer based focal-plane array at 230 GHz," in 26th International Symposium on Space Terahertz Technology, Mar. 2015.
- D. M. Pozar, Microwave Engineering, 4th ed. Hoboken, NJ: Wiley, 2012.

MIR UPDATE: MIR JUNE2021 RELEASE

MIR JUNE2021 release can now be downloaded for general use from:

https://github.com/qi-molecules/sma-mir

The update includes two major updates:

1) a new program UTI_DOPPLER to apply the Doppler tracking corrections offline. There appears to be a hardware/software issue that causes phase jumps in the cross receiver phases when Doppler earth correction is enabled in the course of a polarization track. Disabling the continuous Doppler corrections has completely eliminated the phase jumps. The new MIR program can be used to apply Doppler tracking corrections for the individual sources offline. The figure below shows the spectra of the H30α line (231.90093 GHz) and H31α line (210.501771 GHz) towards a young star MWC 349A and the line velocity after the MIR offline correction is consistent with what is published in Zhang et al. (2017).

Zhang, Q., Claus, B., Watson, L., et al. 2017, ApJ, 837, 53

2) a new program MIR2MS to convert MIR data to CASA measurement sets. The program makes use of the new v4 data headers and converts the visibility data into a true TOPO frame, like ALMA and VLA use. Then it will produce a fully concatenated measurement set, by first concatenating each spw of a target into a target measurement set, then concatenating all targets. This will allow a full calibration in CASA for SMA data.

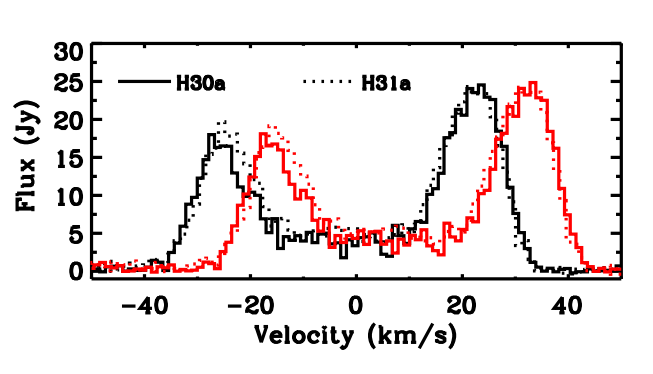

Figure 1: The data with Doppler tracking disabled are shown in black color. The velocity corrected lines (shown in red) are consistent with what is published in Zhang et al. 2017.

LINKS

A more formal introduction to MIR:

https://www.cfa.harvard.edu/rtdc/SMAdata/process/mir/

The MIR Cookbook for use cases:

http://www.cfa.harvard.edu/~cqi/mircook.html

2021 SUBMILLIMETER ARRAY INTERFEROMETRY SCHOOL

The Center for Astrophysics, in conjunction with the Academia Sinica Institute of Astronomy and Astrophysics and the University of Hawaii, held the Submillimeter Array Interferometry School from March 14 - 19, 2021. The school was conducted virtually, with instructors joining in from across the globe. The SMA Interferometry School aims to provide advanced undergraduates, graduate students, post-docs and early career scientists outside the field with a broad knowledge of interferometry and data reduction techniques at millimeter and submillimeter wavelengths.

This year, students were trained through a mixture of lectures, online discussion sessions, group data reduction training sessions, and observing projects. Though the weather was not always cooperative, a majority of the students were able to conduct observations on a wide array of astronomical targets, from local star-forming regions to high-redshift galaxies. This year's school hosted a total of 35 students from 32 different institutions and 15 different countries.

Presentations from the lectures of the school, include slides and recording, can be found here:.

https://www.cfa.harvard.edu/sma-school/program

The organizing committee wishes to thank all those who helped to put on the school, as well as all those who attended. Those who are interested in participating in the SMA Interferometry School in the future are encouraged to contact **sma-school@cfa.harvard.edu** for further information.

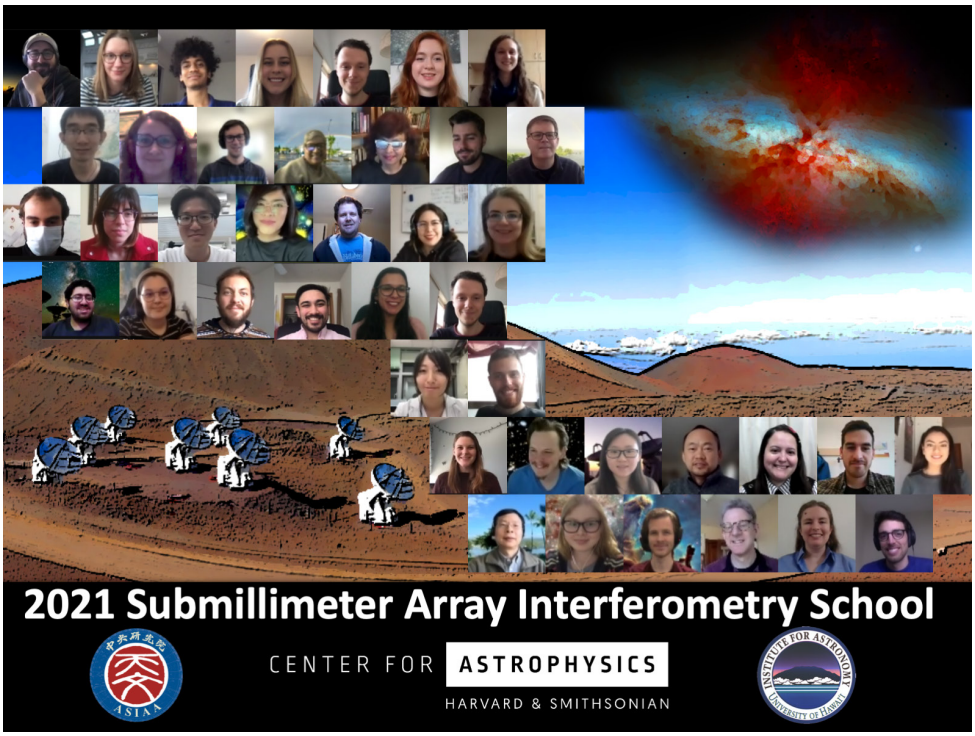

STAFF CHANGES IN HILO

Travis Nelson, Astrophysicist (Telescope Operator), left the SMA at the end of March to pursue other opportunities. We thank Travis for his efforts and wish him success in the future.

SMA POSTDOCTORAL FELLOWS: COMINGS AND GOINGS

The Submillimeter Array Postdoctoral Fellowship program supports early career scientists active in a variety of astronomical research fields involving submillimeter astronomy. The SMA Fellowship is competitive, and a high percentage of our past Fellows have gone on to permanent faculty and research staff positions located around the world.

The SMA welcomes our newest Fellow:

Sara Issaoun is finishing her Ph.D. work at Radboud University, Netherlands, with the thesis 'Imaging Black Hole Inner Accretion Flows with Very Long Baseline Interferometry' (advisor: Dr. Heino Falcke). Sara's research is focused on black holes, accretion flow mechanisms, computational imaging, and very long baseline interferometry. She will join the Center for Astrophysics in 2021 as an NHFP (NASA Hubble Fellowship Program) Einstein Fellow and is expected to take up the SMA fellowship after the completion of the Einstein Fellowship.

As the new Fellow arrives, we also take the time to thank **Andrew Burkhardt** who moved to Wellesley College recently to take up a visiting lectureship position in Physics. There, he will teach and mentor undergraduate students while continuing his research on astrochemistry.

We wish all our current and former Fellowship holders continued success!

A list of current and former SMA Fellows is provided at **https://www.cfa.harvard.edu/opportunities/fellowships/sma/smafellows.html** along with further information on the SMA Fellowship program, including announcement of future SMA Fellowship opportunities.

Qizhou Zhang
Chair, SMA Fellowship Selection Committee

CALL FOR STANDARD OBSERVING PROPOSALS - 2021B SEMESTER

We wish to draw your attention to the next Call for Standard Observing Proposals for observations with the Submillimeter Array (SMA). This call is for the 2021B semester with observing period **16 Nov 2021 - 15 May 2022.**

Standard Observing Proposals Submission deadline: **Thursday, 16 September 2021 20:00 GMT**

The full Call for Proposals, with details on time available and the proposal process, will be available by **August 16** at the SMA Observer Center (SMAOC) at **http://sma1.sma.hawaii.edu/call.html.**

Details on the SMA capabilities and status can be found at **http://sma1.sma.hawaii.edu/status.html;** proposal creation and submission is also done through the SMAOC at **http://sma1.sma.hawaii.edu/proposing.html.** We are happy to answer and questions and provide assistance in proposal submission, simply email sma-propose@cfa.harvard.edu with any inquiries.

Sincerely,

Mark Gurwell
SAO Chair, SMA TAC

Hau-Yu (Baobab) Liu
ASIAA Chair, SMA TAC

PROPOSAL STATISTICS 2020B (2021 JUN 01 – 2021 NOV 15)

The SMA partner institutions received a total of 74 proposals (SAO 65, ASIAA 7, UHawaii 2) requesting observing time in the 2021A semester. The 72 proposals from SAO and ASIAA reviewed by the joint SAO and ASIAA Time Allocation Committee are divided among science categories as follows:

CATEGORY	PROPOSALS
high mass (OB) star formation, cores	16
local galaxies, starbursts, AGN	16
low/intermediate mass star formation, cores	12
protoplanetary, transition, debris disks	8
submm/hi-z galaxies	8
evolved stars, AGB, PPN	6
GRB, SN, high energy	4
UH	2
other	1
solar system	1

TRACK ALLOCATIONS BY WEATHER REQUIREMENT (ALL PARTNERS):

PWV[1]	SAO	ASIAA	UH[2]
< 4.0mm	21A + 49B	4A + 13B	0
< 2.5mm	19A + 28B	1A + 0B	4
< 1.0mm	0A + 0B	2A + 0B	0
Total	**40A + 77B**	**7A + 13B**	**4**

(1) Precipitable water vapor required for the observations.

(2) UH does not list As and Bs.

TOP-RANKED 2021A SEMESTER PROPOSALS

The following is the listing of all SAO and ASIAA proposals with at least a partial A ranking with the names and affiliations of the principal investigators.

GRB, SN, HIGH ENERGY

Deanne Coppejans, Northwestern University
Constraining the Nature and Progenitors of the Fast Blue Optical Transients

Yuji Urata, NCU
Electro-magnetic wave candidate of IceCube Neutrino event

Yuji Urata, NCU
Jet Structures of Gamma-Ray Bursts

HIGH MASS (OB) STAR FORMATION, CORES

Han-Tsung Lee, ASIAA/NCU
Magnetic field in fragmented cores

Henrik Beuther, Max-Planck-Institute for Astronomy
The importance of magnetic fields for the fragmentation of high-mass star-forming regions (the remaining targets)

Qizhou Zhang, CfA
Magnetic Fields and protocluster formation

Todd Hunter, NRAO
Triggered follow-up of accretion outbursts in massive protostars (2021A)

LOCAL GALAXIES, STARBURSTS, AGN

Deanne Fisher, Swinburne University
Testing Feedback Theory in Starbursting Disk Galaxies

Eric Koch, CfA
A resolved molecular gas survey of the edge-on galaxy NGC 891

Eric Koch, CfA
Resolving the molecular gas fuelling IC 10's starburst on 2.5 pc scales

Gerrit Schellenberger, Smithsonian Astrophysical Observatory
Understanding the Time Variability of the AGN in NGC 5044

Matthew Ashby, Harvard-Smithsonian Center for Astrophysics
Measuring H2 Conversion Factors and Physical Conditions in GMCs

Steven Willner, CfA
Disentangling radiating particle properties and jet physics from M87 multi-wavelength variability

Tirna Deb, Kapteyn Astronomical Institute, University of Groningen, NL
SYMPHANY: SYnergy of Molecular PHase And Neutral hYdrogen in galaxies in Abell 2626

Venkatessh Ramakrishnan, University of Concepcion
Polarimetric monitoring of the flaring blazar 1156+295

LOW/INTERMEDIATE MASS STAR FORMATION, CORES

Chat Hull, National Astronomical Observatory of Japan
Cepheus Polarization Pilot Survey

Chin-Fei Lee, ASIAA
Searching for outflows in a very short time-scale sporadic-accretion brown dwarf

Logan Francis, University of Victoria
Completing SMA Monitoring of the periodic outbursting protostar EC53

PROTOPLANETARY, TRANSITION, DEBRIS DISKS

David Wilner, CfA
An Imaging Survey of Forgotten Nearby Herbig Ae/Be Stars

Jun Hashimoto, Astrobiology Center
Giant cavity around very low mass star 2MASS J04351455-1414468

SUBMM/HI-Z GALAXIES

Giovanni G. Fazio, Harvard Smithsonian Center for Astrophysics
Understanding the Evolution of Obscured Activity Over Cosmic Time: A Pilot Survey in the JWST Time Domain Field

STANDARD AND LARGE SCALE PROJECTS OBSERVED DURING 2020B

SMA Semester 2020B encompassed the period 16 Nov 2020 – 30 May 2021 (was 15 May 2021). Hardware failures for two antennas and the transporter during March led to a 15 day lengthening of the semester in an effort to recoup some observing time for affected projects. Unavoidably, though, operational efficiency was lower in the 2nd half of the semester. Nonetheless, it was a successful semester with many completed projects. In addition, one SAO large scale program was allocated significant time in November and December. Listed below are all SMA standard and large scale projects that were at least partially completed during the SMA Semester 2020B.

Mojegan Azadi, CfA
The Emission Mechanisms in the Progenitors of Massive Present-Day Ellipticals

Sara Beck, Tel Aviv University
Molecular Outflow and a Hot Superbubble in Haro 2 (copied from 2020A-S004)

Yue Cao, CfA
Primordial fragmentation of high-mass star formation in 70 um-dark cores

Jaclyn Champagne, University of Texas at Austin
Searching for the Cores of the Most Massive Galaxy Protoclusters at 2<z<3

David Clements, Imperial College London
Extreme Starbursts - the most rapidly star-forming galaxies in the universe (copied from 2019B-S003) (copied from 2020A-S005)

Lennox Cowie, University of Hawaii
A Uniquely Massively Star-forming Protocluster at z=3.15 in the GOODS-N

Logan Francis, University of Victoria
SMA Monitoring of the periodic outbursting protostar EC53

Seiji Fujimoto, Casmic Dawn Center
A Vigorously Star-forming Red Quasar Firstly Discovered at z>7

Kirsten Hall, CfA
Constraining dust spectra and detecting hot quasar winds via the thermal Sunyaev-Zel'dovich Effect, Part 2

Jason Hinkle, University of Hawaii
Rainbow tide: multi-wavelength follow-up of tidal disruption events

Naomi Hirano, ASIAA
Variability and proper motion of the L1448C(N) protostellar jet

Anna Ho, UC Berkeley
Long-lived, luminous millimeter transients from engine-powered stellar explosions in dense environments

Kuiyun Huang, CYCU
Multi-frequency follow-ups of Short GRBs

Maria Jesus Jimenez-Donaire, CfA
Searching for Embedded Super Star Clusters in M82

Garrett Karto Keating, CfA
The Millimeter-wave Intensity Mapping Experiment (mmIME) Large Scale Program

Garrett Karto Keating, CfA
Polarimetric VLBI with the Event Horizon Telescope

Rohit Kondapally, University of Edinburgh
Revealing the nature of the most extreme, dusty, LOFAR-identified galaxies at 3<z<5

Romane Le Gal, CfA
Sulfur Chemistry in Planet-forming Disks

Feng Long, CfA
Mapping the Gas Environment of Heavily Veiled Young Stars

Xing Lu, National Astronomical Observatory of Japan
Tracing the Gas Flow in High-mass Star Forming Filaments

Hugo Messias, Joint ALMA Observatory
Identifying the foreground absorber in PKS0347-211's line of sight

Jamila Pegues, CfA
SMA Survey of Chemistry in Herbig Ae/Be Protoplanetary Disks

Giulia Perotti, University of Copenhagen
Mind the gap: linking ice and gas around R CrA (DDT for 2020B)

Charlie Qi, CfA
Resolving the gas vertical structure of edge-on protoplanetary disks

Allison Towner, University of Florida
Characterizing MYSO Accretion-Outburst Candidates with the SMA

Abygail Waggoner, University of Virginia
Was Variable ION Chemistry in the IM LUP Planet-Forming Disk caused by Stellar X-Ray Flares?

Wei-Hao Wang, ASIAA
SMA STUDIES II: Unidentified SCUBA-2 Sources

Jonathan Williams, University of Hawaii
Early Planet Formation in Embedded Disks

Ya-Lin Wu, National Taiwan Normal University
Probing the Giant Molecular Clouds in NGC 5055

Qizhou Zhang, CfA
Magnetic Fields and protocluster formation

RECENT PUBLICATIONS

TITLE: The Photometric and Spectroscopic Evolution of Rapidly Evolving Extragalactic Transients in ZTF
AUTHOR: Ho, Anna Y. Q.; Perley, Daniel A.; Gal-Yam, Avishay; Lunnan, Ragnhild; Sollerman, Jesper; Schulze, Steve; Das, Kaustav K.; Dobie, Dougal; Yao, Yuhan; Fremling, Christoffer; Adams, Scott; Anand, Shreya; Andreoni, Igor; Bellm, Eric C.; Bruch, Rachel J.; Burdge, Kevin B.; Castro-Tirado, Alberto J.; Dahiwale, Aishwarya; De, Kishalay; Dekany, Richard Drake, Andrew J.; Duev, Dmitry A.; Graham, Matthew J.; Helou, George; Kaplan, David L.; Karambelkar, Viraj; Kasliwal, Mansi M.; Kool, Erik C.; Kulkarni, S. R.; Mahabal, Ashish A.; Medford, Michael S.; Miller, A. A.; Nordin, Jakob; Ofek, Eran; Petitpas, Glen; Riddle, Reed; Sharma, Yashvi; Smith, Roger; Stewart, Adam J.; Taggart, Kirsty; Tartaglia, Leonardo; Tzanidakis, Anastasios; Winters, Jan Martin
PUBLICATION: *eprint arXiv:2105.08811*
PUBLICATION DATE: May 2021
ABSTRACT: https://ui.adsabs.harvard.edu/abs/2021arXiv210508811H/abstract

---

TITLE: Convergent Filaments Contracting Towards an Intermediate-mass Prestellar Core
AUTHOR: Ren, Zhiyuan; Zhu, Lei; Shi, Hui; Yue, Nannan; Li, Di; Zhang, Qizhou; Mardones, Diego; Wu, Jingwen; Jiao, Sihan; Liu, Shu; Luo, Gan; Xie, Jinjin; Zhang, Chao; Xu, Xuefang
PUBLICATION: *eprint arXiv:2105.04116*
PUBLICATION DATE: May 2021
ABSTRACT: https://ui.adsabs.harvard.edu/abs/2021arXiv210504116R/abstract

---

TITLE: The Architecture of the V892 Tau System: the Binary and its Circumbinary Disk
AUTHOR: Long, Feng; Andrews, Sean M.; Vega, Justin; Wilner, David J.; Chandler, Claire J.; Ragusa, Enrico; Teague, Richard; Pérez, Laura M.; Calvet, Nuria; Carpenter, John M.; Henning, Thomas; Kwon, Woojin; Linz, Hendrik; Ricci, Luca
PUBLICATION: *eprint arXiv:2105.02918*
PUBLICATION DATE: May 2021
ABSTRACT: https://ui.adsabs.harvard.edu/abs/2021arXiv210502918L/abstract

---

TITLE: Linking ice and gas in the Lambda Orionis Barnard 35A cloud
AUTHOR: Perotti, G.; Jørgensen, J. K.; Fraser, H. J.; Suutarinen, A. N.; Kristensen, L. E.; Rocha, W. R. M.; Bjerkeli, P.; Pontoppidan, K. M.
PUBLICATION: *eprint arXiv:2105.00652*
PUBLICATION DATE: May 2021
ABSTRACT: https://ui.adsabs.harvard.edu/abs/2021arXiv210500652P/abstract

---

TITLE: Constraints on black-hole charges with the 2017 EHT observations of M87*

AUTHOR: Kocherlakota, Prashant; Rezzolla, Luciano; Falcke, Heino; Fromm, Christian M.; Kramer, Michael; Mizuno, Yosuke; Nathanail, Antonios; Olivares, Héctor; Younsi, Ziri; Akiyama, Kazunori; Alberdi, Antxon; Alef, Walter; Algaba, Juan Carlos; Anantua, Richard; Asada, Keiichi; Azulay, Rebecca; Baczko, Anne-Kathrin; Ball, David; Baloković, Mislav; Barrett, John Benson, Bradford A.; Bintley, Dan; Blackburn, Lindy; Blundell, Raymond; Boland, Wilfred; Bouman, Katherine L.; Bower, Geoffrey C.; Boyce, Hope; Bremer, Michael; Brinkerink, Christiaan D.; Brissenden, Roger; Britzen, Silke; Broderick, Avery E.; Broguiere, Dominique; Bronzwaer, Thomas; Byun, Do-Young; Carlstrom, John E.; Chael, Andrew; Chan, Chi-kwan; Chatterjee, Shami; Chatterjee, Koushik; Chen, Ming-Tang; Chen, Yongjun; Chesler, Paul M.; Cho, Ilje; Christian, Pierre; Conway, John E.; Cordes, James M.; Crawford, Thomas M.; Crew, Geoffrey B.; Cruz-Osorio, Alejandro; Cui, Yuzhu; Davelaar, Jordy; De Laurentis, Mariafelicia; Deane, Roger; Dempsey, Jessica; Desvignes, Gregory; Doeleman, Sheperd S.; Eatough, Ralph P.; Farah, Joseph; Fish, Vincent L.; Fomalont, Ed; Fraga-Encinas, Raquel; Friberg, Per; Ford, H. Alyson; Fuentes, Antonio; Galison, Peter; Gammie, Charles F.; García, Roberto; Gentaz, Olivier; Georgiev, Boris; Goddi, Ciriaco; Gold, Roman; Gómez, José L.; Gómez-Ruiz, Arturo I.; Gu, Minfeng; Gurwell, Mark; Hada, Kazuhiro; Haggard, Daryl; Hecht, Michael H.; Hesper, Ronald; Ho, Luis C.; Ho, Paul; Honma, Mareki; Huang, Chih-Wei L.; Huang, Lei; Hughes, David H.; Ikeda, Shiro; Inoue, Makoto; Issaoun, Sara; James, David J.; Jannuzi, Buell T.; Janssen, Michael; Jeter, Britton; Jiang, Wu; Jimenez-Rosales, Alejandra; Johnson, Michael D.; Jorstad, Svetlana; Jung, Taehyun; Karami, Mansour; Karuppusamy, Ramesh; Kawashima, Tomohisa; Keating, Garrett K.; Kettenis, Mark; Kim, Dong-Jin; Kim, Jae-Young; Kim, Jongsoo; Kim, Junhan; Kino, Motoki; Koay, Jun Yi; Kofuji, Yutaro; Koch, Patrick M.; Koyama, Shoko; Kramer, Carsten; Krichbaum, Thomas P.; Kuo, Cheng-Yu; Lauer, Tod R.; Lee, Sang-Sung; Levis, Aviad; Li, Yan-Rong; Li, Zhiyuan; Lindqvist, Michael; Lico, Rocco; Lindahl, Greg; Liu, Jun; Liu, Kuo; Liuzzo, Elisabetta; Lo, Wen-Ping; Lobanov, Andrei P.; Loinard, Laurent; Lonsdale, Colin; Lu, Ru-Sen; MacDonald, Nicholas R.; Mao, Jirong; Marchili, Nicola; Markoff, Sera; Marrone, Daniel P.; Marscher, Alan P.; Martí-Vidal, Iván; Matsushita, Satoki; Matthews, Lynn D.; Medeiros, Lia; Menten, Karl M.; Mizuno, Izumi; Moran, James M.; Moriyama, Kotaro; Moscibrodzka, Monika; Müller, Cornelia; Musoke, Gibwa; Mejías, Alejandro Mus; Nagai, Hiroshi; Nagar, Neil M.; Nakamura, Masanori; Narayan, Ramesh; Narayanan, Gopal; Natarajan, Iniyan; Neilsen, Joseph; Neri, Roberto; Ni, Chunchong; Noutsos, Aristeidis; Nowak, Michael A.; Okino, Hiroki; Ortiz-León, Gisela N.; Oyama, Tomoaki; Özel, Feryal; Palumbo, Daniel C. M.; Park, Jongho; Patel, Nimesh; Pen, Ue-Li; Pesce, Dominic W.; Piétu, Vincent; Plambeck, Richard; PopStefanija, Aleksandar; Porth, Oliver; Pötzl, Felix M.; Prather, Ben; Preciado-López, Jorge A.; Psaltis, Dimitrios; Pu, Hung-Yi; Ramakrishnan, Venkatessh; Rao, Ramprasad; Rawlings, Mark G.; Raymond, Alexander W.; Ricarte, Angelo; Ripperda, Bart; Roelofs, Freek; Rogers, Alan; Ros, Eduardo; Rose, Mel; Roshanineshat, Arash; Rottmann, Helge; Roy, Alan L.; Ruszczyk, Chet; Rygl, Kazi L. J.; Sánchez, Salvador; Sánchez-Arguelles, David; Sasada, Mahito; Savolainen, Tuomas; Schloerb, F. Peter; Schuster, Karl-Friedrich; Shao, Lijing; Shen, Zhiqiang; Small, Des; Sohn, Bong Won; SooHoo, Jason; Sun, He; Tazaki, Fumie; Tetarenko, Alexandra J.; Tiede, Paul; Tilanus, Remo P. J.; Titus, Michael; Toma, Kenji; Torne, Pablo; Trent, Tyler; Traianou, Efthalia; Trippe, Sascha; van Bemmel, Ilse; van Langevelde, Huib Jan; van Rossum, Daniel R.; Wagner, Jan; Ward-Thompson, Derek; Wardle, John; Weintroub, Jonathan; Wex, Norbert; Wharton, Robert; Wielgus, Maciek; Wong, George N.; Wu, Qingwen; Yoon, Doosoo; Young, André; Young, Ken; Yuan, Feng; Yuan, Ye-Fei; Zensus, J. Anton; Zhao, Guang-Yao; Zhao, Shan-Shan; EHT Collaboration

PUBLICATION: *Physical Review D, Volume 103, Issue 10, article id.104047*

PUBLICATION DATE: May 2021

ABSTRACT: https://ui.adsabs.harvard.edu/abs/2021PhRvD.103j4047K/abstract

---

TITLE: Evolutions of CH 3 CN abundance in molecular clumps

AUTHOR: He, Zhen-Zhen; Li, Guang-Xing; Zhang, Chao

PUBLICATION: *eprint arXiv:2104.06810*

PUBLICATION DATE: April 2021

ABSTRACT: https://ui.adsabs.harvard.edu/abs/2021arXiv210406810H/abstract

---

TITLE: Broadband Multi-wavelength Properties of M87 during the 2017 Event Horizon Telescope Campaign

AUTHOR: Algaba, J. C.; Anczarski, J.; Asada, K.; Balokovic, M.; Chandra, S.; Cui, Y. -Z.; Falcone, A. D.; Giroletti, M.; Goddi, C.; Hada, K.; Haggard, D.; Jorstad, S.; Kaur, A.; Kawashima, T.; Keating, G.; Kim, J. -Y.; Kino, M.; Komossa, S.; Kravchenko, E. V.; Krichbaum, T. P. Lee, S. -S.; Lu, R. -S.; Lucchini, M.; Markoff, S.; Neilsen, J.; Nowak, M. A.; Park, J.; Principe, G.; Ramakrishnan, V.; Reynolds, M. T.; Sasada, M.; Savchenko, S. S.; Williamson, K. E.; The Event Horizon Telescope Collaboration; The Fermi Large Area Telescope Collaboration; H. E. S. S. Collaboration; MAGIC Collaboration; VERITAS Collaboration; EAVN Collaboration

PUBLICATION: *eprint arXiv:2104.06855*

PUBLICATION DATE: April 2021

ABSTRACT: https://ui.adsabs.harvard.edu/abs/2021arXiv210406855A/abstract

---

TITLE: The Extraordinary Outburst in the Massive Protostellar System NGC 6334 I-MM1: Strong Increase in Mid-Infrared Continuum Emission

AUTHOR: Hunter, T. R.; Brogan, C. L.; De Buizer, J. M.; Towner, A. P. M.; Dowell, C. D.; MacLeod, G. C.; Stecklum, B.; Cyganowski, C. J.; El-Abd, S. J.; McGuire, B. A.

PUBLICATION: *The Astrophysical Journal Letters, Volume 912, Issue 1, id.L17, 8 pp.*

PUBLICATION DATE: May 2021

ABSTRACT: https://ui.adsabs.harvard.edu/abs/2021ApJ...912L..17H/abstract

---

TITLE: Discovery of an Edge-on Circumstellar Debris Disk Around BD+45 ◦ 598: a Newly Identifed Member of the β Pictoris Moving Group

AUTHOR: Hinkley, Sasha; Matthews, Elisabeth C.; Lefevre, Charlène; Lestrade, Jean-Francois; Kennedy, Grant; Mawet, Dimitri; Stapelfeldt, Karl R.; Ray, Shrishmoy; Mamajek, Eric; Bowler, Brendan P.; Wilner, David; Williams, Jonathan; Ansdell, Megan; Wyatt, Mark; Lau, Alexis; Fernandez Fernandez, Mark W. Phillips Jorge; Gagné, Jonathan; Bubb, Emma; Sutlieff, Ben J.; Wilson, Thomas J. G. Matthews, Brenda; Ngo, Henry; Piskorz, Danielle; Crepp, Justin R.; Gonzalez, Erica; Mann, Andrew W.; Mace, Gregory

PUBLICATION: *eprint arXiv:2103.12824*

PUBLICATION DATE: March 2021

ABSTRACT: https://ui.adsabs.harvard.edu/abs/2021arXiv210312824H/abstract

---

TITLE: First M87 Event Horizon Telescope Results. VIII. Magnetic Field Structure near The Event Horizon

AUTHOR: Event Horizon Telescope Collaboration; Akiyama, Kazunori; Algaba, Juan Carlos; Alberdi, Antxon; Alef, Walter; Anantua, Richard; Asada, Keiichi; Azulay, Rebecca; Baczko, Anne-Kathrin; Ball, David; Baloković, Mislav; Barrett, John; Benson, Bradford A.; Bintley, Dan; Blackburn, Lindy; Blundell, Raymond; Boland, Wilfred; Bouman, Katherine L.; Bower, Geoffrey C.; Boyce, Hope; Brinkerink, Christiaan D.; Brissenden, Roger; Britzen, Silke; Broderick, Avery E.; Broguiere, Dominique; Bronzwaer, Thomas; Byun, Do-Young; Carlstrom, John E.; Chael, Andrew; Chan, Chi-kwan; Chatterjee, Shami; Chatterjee, Koushik; Chen, Ming-Tang; Chen, Yongjun; Chesler, Paul M.; Cho, Ilje; Christian, Pierre; Conway, John E.; Cordes, James M.; Crawford, Thomas M.; Crew, Geoffrey B.; Cruz-Osorio, Alejandro; Cui, Yuzhu; Davelaar, Jordy; De Laurentis, Mariafelicia; Deane, Roger; Dempsey, Jessica; Desvignes, Gregory; Dexter, Jason; Doeleman, Sheperd S.; Eatough, Ralph P.; Falcke, Heino; Farah, Joseph; Fish, Vincent L.; Fomalont, Ed; Ford, H. Alyson; Fraga-Encinas, Raquel; Friberg, Per; Fromm, Christian M.; Fuentes, Antonio; Galison, Peter; Gammie, Charles F.; García, Roberto; Gelles, Zachary; Gentaz, Olivier; Georgiev, Boris; Goddi, Ciriaco; Gold, Roman; Gómez, José L.; Gómez-Ruiz, Arturo I.; Gu, Minfeng; Gurwell, Mark; Hada, Kazuhiro; Haggard, Daryl; Hecht, Michael H.; Hesper, Ronald; Himwich, Elizabeth; Ho, Luis C.; Ho, Paul; Honma, Mareki; Huang, Chih-Wei L.; Huang, Lei; Hughes, David H.; Ikeda, Shiro; Inoue, Makoto; Issaoun, Sara; James, David J.; Jannuzi, Buell T.; Janssen, Michael; Jeter, Britton; Jiang, Wu; Jimenez-Rosales, Alejandra; Johnson, Michael D.; Jorstad, Svetlana; Jung, Taehyun; Karami, Mansour; Karuppusamy, Ramesh; Kawashima, Tomohisa; Keating, Garrett K.; Kettenis, Mark; Kim, Dong-Jin; Kim, Jae-Young; Kim, Jongsoo; Kim, Junhan; Kino, Motoki; Koay, Jun Yi; Kofuji, Yutaro; Koch, Patrick M.; Koyama, Shoko; Kramer, Michael; Kramer, Carsten; Krichbaum, Thomas P.; Kuo, Cheng-Yu; Lauer, Tod R.; Lee, Sang-Sung; Levis, Aviad; Li, Yan-Rong; Li, Zhiyuan; Lindqvist, Michael; Lico, Rocco; Lindahl, Greg; Liu, Jun; Liu, Kuo; Liuzzo, Elisabetta; Lo, Wen-Ping; Lobanov, Andrei P.; Loinard, Laurent; Lonsdale, Colin; Lu, Ru-Sen; MacDonald, Nicholas R.; Mao, Jirong; Marchili,

Nicola; Markoff, Sera; Marrone, Daniel P.; Marscher, Alan P.; Martí-Vidal, Iván; Matsushita, Satoki; Matthews, Lynn D.; Medeiros, Lia; Menten, Karl M.; Mizuno, Izumi; Mizuno, Yosuke; Moran, James M.; Moriyama, Kotaro; Moscibrodzka, Monika; Müller, Cornelia; Musoke, Gibwa; Mus Mejías, Alejandro; Michalik, Daniel; Nadolski, Andrew; Nagai, Hiroshi; Nagar, Neil M.; Nakamura, Masanori; Narayan, Ramesh; Narayanan, Gopal; Natarajan, Iniyan; Nathanail, Antonios; Neilsen, Joey; Neri, Roberto; Ni, Chunchong; Noutsos, Aristeidis; Nowak, Michael A.; Okino, Hiroki; Olivares, Héctor; Ortiz-León, Gisela N.; Oyama, Tomoaki; Özel, Feryal; Palumbo, Daniel C. M.; Park, Jongho; Patel, Nimesh; Pen, Ue-Li; Pesce, Dominic W.; Piétu, Vincent; Plambeck, Richard; PopStefanija, Aleksandar; Porth, Oliver; Pötzl, Felix M.; Prather, Ben; Preciado-López, Jorge A.; Psaltis, Dimitrios; Pu, Hung-Yi; Ramakrishnan, Venkatessh; Rao, Ramprasad; Rawlings, Mark G.; Raymond, Alexander W.; Rezzolla, Luciano; Ricarte, Angelo; Ripperda, Bart; Roelofs, Freek; Rogers, Alan; Ros, Eduardo; Rose, Mel; Roshanineshat, Arash; Rottmann, Helge; Roy, Alan L.; Ruszczyk, Chet; Rygl, Kazi L. J.; Sánchez, Salvador; Sánchez-Arguelles, David; Sasada, Mahito; Savolainen, Tuomas; Schloerb, F. Peter; Schuster, Karl-Friedrich; Shao, Lijing; Shen, Zhiqiang; Small, Des; Sohn, Bong Won; SooHoo, Jason; Sun, He; Tazaki, Fumie; Tetarenko, Alexandra J.; Tiede, Paul; Tilanus, Remo P. J.; Titus, Michael; Toma, Kenji; Torne, Pablo; Trent, Tyler; Traianou, Efthalia; Trippe, Sascha; van Bemmel, Ilse; van Langevelde, Huib Jan; van Rossum, Daniel R.; Wagner, Jan; Ward-Thompson, Derek; Wardle, John; Weintroub, Jonathan; Wex, Norbert; Wharton, Robert; Wielgus, Maciek; Wong, George N.; Wu, Qingwen; Yoon, Doosoo; Young, André; Young, Ken; Younsi, Ziri; Yuan, Feng; Yuan, Ye-Fei; Zensus, J. Anton; Zhao, Guang-Yao; Zhao, Shan-Shan

PUBLICATION: *The Astrophysical Journal Letters, Volume 910, Issue 1, id.L13, 43 pp.*

PUBLICATION DATE: March 2021

ABSTRACT: https://ui.adsabs.harvard.edu/abs/2021ApJ...910L..13E/abstract

---

TITLE: First M87 Event Horizon Telescope Results. VII. Polarization of the Ring

AUTHOR: Event Horizon Telescope Collaboration; Akiyama, Kazunori; Algaba, Juan Carlos; Alberdi, Antxon; Alef, Walter; Anantua, Richard; Asada, Keiichi; Azulay, Rebecca; Baczko, Anne-Kathrin; Ball, David; Baloković, Mislav; Barrett, John; Benson, Bradford A.; Bintley, Dan; Blackburn, Lindy; Blundell, Raymond; Boland, Wilfred; Bouman, Katherine L.; Bower, Geoffrey C.; Boyce, Hope; Brinkerink, Christiaan D.; Brissenden, Roger; Britzen, Silke; Broderick, Avery E.; Broguiere, Dominique; Bronzwaer, Thomas; Byun, Do-Young; Carlstrom, John E.; Chael, Andrew; Chan, Chi-kwan; Chatterjee, Shami; Chatterjee, Koushik; Chen, Ming-Tang; Chen, Yongjun; Chesler, Paul M.; Cho, Ilje; Christian, Pierre; Conway, John E.; Cordes, James M.; Crawford, Thomas M.; Crew, Geoffrey B.; Cruz-Osorio, Alejandro; Cui, Yuzhu; Davelaar, Jordy; De Laurentis, Mariafelicia; Deane, Roger; Dempsey, Jessica; Desvignes, Gregory; Dexter, Jason; Doeleman, Sheperd S.; Eatough, Ralph P.; Falcke, Heino; Farah, Joseph; Fish, Vincent L.; Fomalont, Ed; Ford, H. Alyson; Fraga-Encinas, Raquel; Freeman, William T.; Friberg, Per; Fromm, Christian M.; Fuentes, Antonio; Galison, Peter; Gammie, Charles F.; García, Roberto; Gentaz, Olivier; Georgiev, Boris; Goddi, Ciriaco; Gold, Roman; Gómez, José L.; Gómez-Ruiz, Arturo I.; Gu, Minfeng; Gurwell, Mark; Hada, Kazuhiro; Haggard, Daryl; Hecht, Michael H.; Hesper, Ronald; Ho, Luis C.; Ho, Paul; Honma, Mareki; Huang, Chih-Wei L.; Huang, Lei; Hughes, David H.; Ikeda, Shiro; Inoue, Makoto; Issaoun, Sara; James, David J.; Jannuzi, Buell T.; Janssen, Michael; Jeter, Britton; Jiang, Wu; Jimenez-Rosales, Alejandra; Johnson, Michael D.; Jorstad, Svetlana; Jung, Taehyun; Karami, Mansour; Karuppusamy, Ramesh; Kawashima, Tomohisa; Keating, Garrett K.; Kettenis, Mark; Kim, Dong-Jin; Kim, Jae-Young; Kim, Jongsoo; Kim, Junhan; Kino, Motoki; Koay, Jun Yi; Kofuji, Yutaro; Koch, Patrick M.; Koyama, Shoko; Kramer, Michael; Kramer, Carsten; Krichbaum, Thomas P.; Kuo, Cheng-Yu; Lauer, Tod R.; Lee, Sang-Sung; Levis, Aviad; Li, Yan-Rong; Li, Zhiyuan; Lindqvist, Michael; Lico, Rocco; Lindahl, Greg; Liu, Jun; Liu, Kuo; Liuzzo, Elisabetta; Lo, Wen-Ping; Lobanov, Andrei P.; Loinard, Laurent; Lonsdale, Colin; Lu, Ru-Sen; MacDonald, Nicholas R.; Mao, Jirong; Marchili, Nicola; Markoff, Sera; Marrone, Daniel P.; Marscher, Alan P.; Martí-Vidal, Iván; Matsushita, Satoki; Matthews, Lynn D.; Medeiros, Lia; Menten, Karl M.; Mizuno, Izumi; Mizuno, Yosuke; Moran, James M.; Moriyama, Kotaro; Moscibrodzka, Monika; Müller, Cornelia; Musoke, Gibwa; Mejías, Alejandro Mus; Michalik, Daniel; Nadolski, Andrew; Nagai, Hiroshi; Nagar, Neil M.; Nakamura, Masanori; Narayan, Ramesh; Narayanan, Gopal; Natarajan, Iniyan; Nathanail, Antonios; Neilsen, Joey; Neri, Roberto; Ni, Chunchong; Noutsos, Aristeidis; Nowak, Michael A.; Okino, Hiroki; Olivares, Héctor; Ortiz-León, Gisela N.; Oyama, Tomoaki; Özel, Feryal; Palumbo, Daniel C. M.; Park, Jongho; Patel, Nimesh; Pen, Ue-Li; Pesce, Dominic W.; Piétu, Vincent; Plambeck, Richard; PopStefanija, Aleksandar; Porth, Oliver; Pötzl, Felix M.; Prather, Ben; Preciado-López, Jorge A.; Psaltis, Dimitrios; Pu, Hung-Yi; Ramakrishnan, Venkatessh; Rao, Ramprasad; Rawlings, Mark G.; Raymond, Alexander W.; Rezzolla, Luciano; Ricarte, Angelo; Ripperda, Bart; Roelofs, Freek; Rogers, Alan; Ros, Eduardo; Rose, Mel; Roshanineshat, Arash; Rottmann, Helge; Roy, Alan L.; Ruszczyk, Chet; Rygl, Kazi L.

J.; Sánchez, Salvador; Sánchez-Arguelles, David; Sasada, Mahito; Savolainen, Tuomas; Schloerb, F. Peter; Schuster, Karl-Friedrich; Shao, Lijing; Shen, Zhiqiang; Small, Des; Sohn, Bong Won; SooHoo, Jason; Sun, He; Tazaki, Fumie; Tetarenko, Alexandra J.; Tiede, Paul; Tilanus, Remo P. J.; Titus, Michael; Toma, Kenji; Torne, Pablo; Trent, Tyler; Traianou, Efthalia; Trippe, Sascha; van Bemmel, Ilse; van Langevelde, Huib Jan; van Rossum, Daniel R.; Wagner, Jan; Ward-Thompson, Derek; Wardle, John; Weintroub, Jonathan; Wex, Norbert; Wharton, Robert; Wielgus, Maciek; Wong, George N.; Wu, Qingwen; Yoon, Doosoo; Young, André; Young, Ken; Younsi, Ziri; Yuan, Feng; Yuan, Ye-Fei; Zensus, J. Anton; Zhao, Guang-Yao; Zhao, Shan-Shan

PUBLICATION: *The Astrophysical Journal Letters, Volume 910, Issue 1, id.L12, 48 pp.*
PUBLICATION DATE: March 2021
ABSTRACT: https://ui.adsabs.harvard.edu/abs/2021ApJ...910L..12E/abstract

---

TITLE: Multiwavelength Observations of the RV Tauri Variable System U Monocerotis: Long-term Variability Phenomena That Can Be Explained by Binary Interactions with a Circumbinary Disk
AUTHOR: Vega, Laura D.; Stassun, Keivan G.; Montez, Rodolfo, Jr.; Kamiński, Tomasz; Sabin, Laurence; Schlegel, Eric M.; Vlemmings, Wouter H. T.; Kastner, Joel H.; Ramstedt, Sofia; Boyd, Patricia T.
PUBLICATION: *The Astrophysical Journal, Volume 909, Issue 2, id.138, 14 pp.*
PUBLICATION DATE: March 2021
ABSTRACT: https://ui.adsabs.harvard.edu/abs/2021ApJ...909..138V/abstract

---

TITLE: 25 au Angular Resolution Observations of HH 211 with ALMA: Jet Properties and Shock Structures in SiO, CO, and SO
AUTHOR: Jhan, Kai-Syun; Lee, Chin-Fei
PUBLICATION: *The Astrophysical Journal, Volume 909, Issue 1, id.11, 17 pp.*
PUBLICATION DATE: March 2021
ABSTRACT: https://ui.adsabs.harvard.edu/abs/2021ApJ...909...11J/abstract

---

TITLE: Simultaneous Deep Measurements of CO Isotopologues and Dust Emission in Giant Molecular Clouds in the Andromeda Galaxy
AUTHOR: Viaene, Sébastien; Forbrich, Jan; Lada, Charles J.; Petitpas, Glen; Faesi, Christopher
PUBLICATION: *The Astrophysical Journal, Volume 912, Issue 1, id.68, 17 pp.*
PUBLICATION DATE: May 2021
ABSTRACT: https://ui.adsabs.harvard.edu/abs/2021ApJ...912...68V/abstract

---

TITLE: The Relativistic Jet Orientation and Host Galaxy of the Peculiar Blazar PKS 1413+135
AUTHOR: Readhead, A. C. S.; Ravi, V.; Liodakis, I.; Lister, M. L.; Singh, V.; Aller, M. F.; Blandford, R. D.; Browne, I. W. A.; Gorjian, V.; Grainge, K. J. B.; Gurwell, M. A.; Hodges, M. W.; Hovatta, T.; Kiehlmann, S.; Lähteenmäki, A.; Mcaloone, T.; Max-Moerbeck, W.; Pavlidou, V.; Pearson, T. J.; Peirson, A. L.; Reeves, R. A.; Soifer, B. T.; Taylor, G. B.; Tornikoski, M.; Vedantham, H. K.; Werner, M.; Wilkinson, P. N.; Zensus, J. A.
PUBLICATION: *The Astrophysical Journal, Volume 907, Issue 2, id.61, 24 pp.*
PUBLICATION DATE: February 2021
ABSTRACT: https://ui.adsabs.harvard.edu/abs/2021ApJ...907...61R/abstract

---

TITLE: Molecular remnant of Nova 1670 (CK Vulpeculae). II. A three-dimensional view of the gas distribution and velocity field
AUTHOR: Kamiński, T.; Steffen, W.; Bujarrabal, V.; Tylenda, R.; Menten, K. M.; Hajduk, M.
PUBLICATION: *Astronomy & Astrophysics, Volume 646, id.A1, 11 pp.*
PUBLICATION DATE: February 2021
ABSTRACT: https://ui.adsabs.harvard.edu/abs/2021A%26A...646A...1K/abstract

---

The Submillimeter Array (SMA) is a pioneering radio-interferometer dedicated to a broad range of astronomical studies including finding protostellar disks and outflows; evolved stars; the Galactic Center and AGN; normal and luminous galaxies; and the solar system. Located on Maunakea, Hawaii, the SMA is a collaboration between the Smithsonian Astrophysical Observatory and the Academia Sinica Institute of Astronomy and Astrophysics.

SUBMILLIMETER ARRAY
Center for Astrophysics | Harvard & Smithsonian
60 Garden Street, MS 78
Cambridge, MA 02138 USA
www.cfa.harvard.edu/sma/

SMA HILO OFFICE
645 North A'ohoku Place
Hilo, Hawaii 96720
Ph. 808.961.2920
Fx. 808.961.2921
sma1.sma.hawaii.edu

ACADEMIA SINICA INSTITUTE
OF ASTRONOMY & ASTROPHYSICS
11F of Astronomy-Mathematics Building,
AS/NTU, No. 1, Sec. 4, Roosevelt Road
Taipei 10617
Taiwan R.O.C.
www.asiaa.sinica.edu.tw/